ELSEVIER

Recent advances in visible light-driven water oxidation and reduction in suspension systems

Dan Kong [a], Yun Zheng [b], Marcin Kobielusz [c], Yiou Wang [a], Zhiming Bai [a,d], Wojciech Macyk [c,*], Xinchen Wang [b,*], Junwang Tang [a,*]

[a] Department of Chemical Engineering, University College London, Torrington Place, London WC1E 7JE, UK
[b] State Key Laboratory of Photocatalysis on Energy and Environment, College of Chemistry, Fuzhou University, Fuzhou 350002, China
[c] Faculty of Chemistry, Jagiellonian University, ul. Gronostajowa 2, 30-387 Kraków, Poland
[d] The School of Material Science and Engineering, Beihang University, No. 37 Xueyuan Road, Haidian District, Beijing, China

In order to solve the shortage of sustainable energy and the related concern about combustion of fossil fuels, converting the most abundant solar energy into chemical fuels becomes one of the most promising choices to provide the everlasting and environmentally friendly energy vector along with the minimum impact on environment. Among the methods of converting solar energy into chemical fuels, there is a significant interest in the renewable hydrogen production by photocatalysts from abundant water under visible light irradiation. Therefore, the development of efficient photocatalysts for water reduction and oxidation in a suspension system is the footstone for the development of solar energy conversion. In this review, the fundamental theory of photocatalysis and key factors affecting photocatalysis will be introduced first. Then the new materials development covering inorganic materials (oxides, nitrides and sulfides), carbon-based photocatalysts, and semiconductor-coordination compound photocatalysts developed over the past 10 years will be addressed with discussion about dominating factors in the photochemical process. This review would provide a comprehensive reference to exploring the efficient and novel materials working for the solar energy conversion to affordable and sustainable fuels. Finally, the perspective of the technology is also discussed.

Introduction

With the concern of sustainable supply of natural gas, oil, and coal and more importantly the severe environmental issues caused by the combustion of the fossil fuels, it is very urgent for the society to discover alternative sources of energy which are sustainable, clean, and abundant [1,2]. Among the potential solutions, converting and storage of solar energy into clean energy carrier is the most preferable choice. As the highest mass energy density medium, hydrogen is a promising energy carrier which can be produced via photocatalytic water reduction driven by solar irradiation, thus storing solar energy into the clean medium H_2. In 1972, Honda-Fujishima reported photoelectrochemical water redox on n-type TiO_2 coupled with a Pt counter electrode to produce the equivalent to hydrogen and oxygen separately under light irradiation, thus demonstrating the feasibility of the technology [3]. However, n-type TiO_2 can only absorb ultra-violet (UV) light to excite electrons from the conduction band to the valence band because of its wide band-gap of 3.2 eV [4]. Visible light constitutes about 43% of the solar spectrum, therefore, researchers have paid much attention on developing novel visible light-driven photocatalysts. Therefore, finding suitable photocatalysts for efficient water redox into H_2 and O_2 under visible light irradiation is critical.

In the past decade, many photocatalysts have been found to be used in photocatalytic water reduction or oxidation under UV or visible light, such as TiO_2 [5,6], ZnO [7,8], WO_3 [9,10],

* Corresponding authors.
E-mail address: Tang, J. (junwang.tang@ucl.ac.uk).

https://doi.org/10.1016/j.mattod.2018.04.009

Fe_2O_3 [11,12], CdS [13,14], SnO_2 [15,16], ZrO_2 [17,18], and TaON [19,20]. This area has moved forward rather fast with many new photocatalysts or photocatalytic systems reported recently. There have been a few reviews and books on water reduction and oxidation published with different focuses (e.g., metal oxides, photoelectrodes or junctions) [1,5,21–23]. Recently, a review gave quantitative descriptions of the physical and chemical properties of the photocatalysts to determine which parameters had the most impact on improving the overall photocatalytic performance [23]. Another review emphasized the two distinct approaches to photocatalytic water splitting, one- and two-step photoexcitation routes [22]. The other review highlighted photonic and electrical driven water splitting together with photovoltaic-integrated solar-driven water electrolysis by summarizing thermolytic, electrolytic, photolytic, and biolytic water splitting [21]. These reviews accumulate the knowledge ranging from different fields and use multidisciplinary approaches to fully understand and improve the efficiency of photocatalysis. This review, different from but complementary to those published, focuses on key factors influencing the photocatalytic activity and more importantly very recent development of photocatalytic materials, in particular visible light-driven photocatalysts instead of UV irradiation which have been substantially reviewed, including not only inorganic photocatalysts (oxides, nitrides and sulfides) but also carbon-based semiconductor photocatalysts and semiconductor-coordination compound systems. Furthermore, this review has investigated a wealth of recent reports on the photocatalytic properties of typical visible light-driven photocatalysts working in the suspension system, putting forward the viable routes to increase efficiency and improving stability by facilitating well-placed band offsets and improved charge separation and transfer. This is believed a basis to both photoelectrochemical water splitting and artificial Z-scheme systems.

Herein, a brief overview based on visible light-driven photocatalytic water splitting in a suspension system is first presented. The mechanism of the photocatalysts and the factors influencing photocatalytic activity will be briefly illustrated. The next section of this review presents the recent development of inorganic photocatalyst, including oxides, sulfides, and nitrides for half reaction of photocatalysis and Z-scheme water splitting. After that, carbon-based organic photocatalysts will be described. Following this section, semiconductor-coordination compounds and factors influencing their performance will be illustrated. Finally, viewpoints on the future exploration of new photocatalysts will be discussed.

Mechanism

Fig. 1 shows the main process and the principle of photocatalytic water splitting in semiconductor photocatalysis. The first step is absorption of photons to generate pairs of electrons and holes (I). Afterward these charges will separate and migrate to the reaction sites or recombine (II). Finally, electrons or holes react with water molecules to evolve H_2 or O_2 (III).

The key of the first step is that the energy of incident light should be larger than the optical gap (also commonly referred to as the absorption onset) of the irradiated photocatalyst, resulting in electron excitation from the highest occupied molecular orbital (HOMO, top of the valence band (VB) in a periodic crystal perspective) to the lowest unoccupied molecular orbital (LUMO, bottom of the conduction band (CB)) and the generation of excitons, namely, excited electron-hole pairs. Such excitons can subsequently dissociate into free electrons and holes (where "free" refers to the fact that they are not bound together as part of excitons) through the supply of additional energy, the exciton binding energy. The optical band plus the exciton binding energy is referred to as band gap. Numerous oxide photocatalysts were found to be active for half reactions in the visible region [24,25], which means their bandgap is narrower than 3.10 eV corresponding to the wavelength of visible light ranging from 400 nm to 700 nm. At the same time, the potential of the CB should be more negative than the reduction potential of H_2O/H_2 (0 V *vs.* NHE, pH = 0), while the VB should be more positive than the oxidation potential of O_2/H_2O (1.23 V *vs.* NHE, pH = 0) [1,26]. Therefore, the theoretical minimum band gap for water splitting is 1.23 eV. The width of the band gap and the levels of the CB and VB are extremely important for semiconductor photocatalysts, which is the footstone for the second and the third step.

These free charge carriers can drive redox reaction in photocatalytic water splitting, but also reform excitons in a process

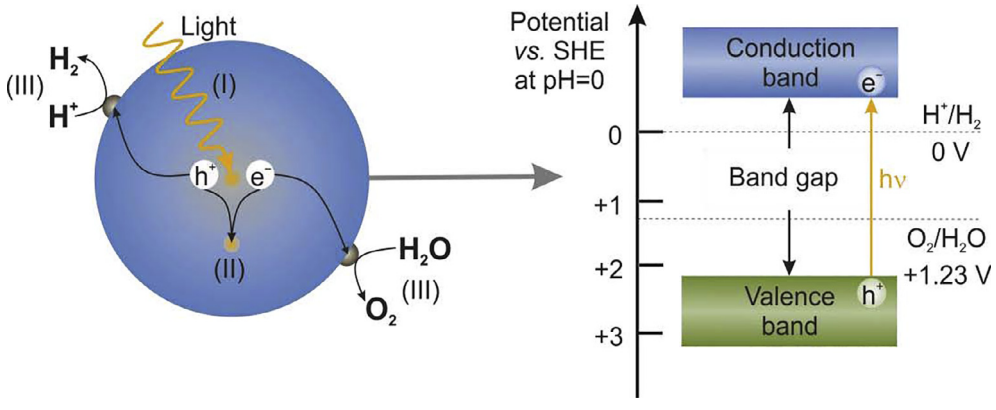

FIGURE 1

The main processes and the principle of photocatalytic water splitting in semiconductor photocatalysts.

commonly referred to as electron-hole recombination. Both free charge carriers and excitons can also become trapped on a part of the photocatalyst, with the defects of the photocatalyst around the free charge carrier or exciton. Excitons, finally, can decay at any stage back to the ground state via fluorescence/phosphorescence, the emission of light, or via internal conversion, a dark nonradiative route, where the excess energy is dissipated in the form of phonons (atomic vibrations). Dynamically, the charge generation is at picosecond timescale and these electrons and holes will be separated and transferred to active sites on the surface of photocatalyst powder at nano- to microsecond timescale, while surface reaction of water splitting is extremely slow at microsecond- to-second timescale due to the slow rate-determining step of O_2 production in the third step [27,28]. Thus, it needs much longer life time of electron-hole pairs to realize efficient water redox reaction on the surface. However, the recombination of charge carriers competes with the last step [27,29]. As a result, it is challenging to keep the life time of electrons and holes long enough along with the recombination of electrons and holes. Here, a co-catalyst can solve this problem as enhancing the charge separation by forming a Schottky junction with semiconductors [30]. For the half reactions of water splitting, appropriate sacrificial reagents can also prevent the recombination of electrons and holes efficiently by extracting one charge carrier, leaving the other to react with water and to produce hydrogen or oxygen [30], as explained in Section "The solution pH".

The reaction rate of the last step is important for the whole photocatalytic process. The reason is not only that the competition of the recombination of charge pairs will reduce the concentration of charges reacted, but also that the desorption rate of the created H_2 or O_2 molecules is much slower, limiting the surface reaction dynamically [28]. In addition, water redox will take place when the practical potential meets the energetic requirements, which has to be much higher than the minimum required to overcome overpotential and other system losses [31]. Therefore, the slowdown of charge recombination is the most important step and improving the surface chemical reactions is highly important in the research field, which has a great meaning for the improvement of the conversion efficiency from solar energy to chemical fuels.

Key factors

According to the main process, there are many factors that influence the photocatalytic performance of semiconductor photocatalysts in water redox, including doping, architecture parameters, cocatalysts, the solution pH, and sacrificial and mediator regents as explained in the following.

Doping

As shown in Fig. 1, when light of high enough energy is used, electrons are promoted from the VB to the CB and the concomitant oxidation and reduction process take place. For the materials, who have bandgaps wider than 3.10 eV as mentioned in Section "Mechanism", are not active under the visible light irradiation, especially for TiO_2, which is among the semiconductors of highest photocatalytic activity but requires irradiation with light of wavelength shorter than the absorption band onset (~350 nm) [32,33]. Thus, metal doping or doping with nonmetallic elements have become an intense research front aimed at expanding the photoresponse of materials with wide bandgaps to the visible region. The more details and the vivid examples about the mental doping in the photocatalysts to enhance the photocatalytic activities [34–39] are shown in Section "Oxide photocatalysts for half reactions". The nonmetal dopants, such as nitrogen (Section "(Oxy)nitride photocatalysts"), sulfide (Section "(Oxy)sulfide photocatalysts"), and carbon (Section "Oxide photocatalysts for half reactions") have been reported to increase the photostability over that of metal-doped catalysts, which could introduce a new energy level above the VB, thus reducing the band gap and increasing the range of light-responsiveness [33]. To a short sum up, doping is an efficient method for extending the light-absorption range of the individual photocatalysts to achieve activity under visible light as well as UV light irradiation.

Architecture parameters

The separation and migration of photogenerated electrons and holes and the surface chemical reaction of H_2 or O_2 evolution are also affected by their architectures, such as morphology, the crystal structure, particle size, and surface area [33,40]. The improvements on the morphology of the photocatalysts can increase the reflection and scattering of incident light among its constituent nanoparticles [33]. For example, Cu_2O with different morphologies such as spherical particles, porous spherical particles, cubes, and octahedral were obtained via adjusting the concentration of NH_3 solution (Fig. 2) [41]. The edge lengths of octahedral could be easily tuned from 130 to 600 nm *via* adjusting the NaOH concentration. The better adsorption ability and photocatalytic ability of these octahedral Cu_2O particles were investigated with the comparison of cubic Cu_2O. Usually, changing the morphology could also adjust the particle size and crystallinity. Photogenerated charges are extremely easy to be trapped and recombine at boundaries and defects. Thus, if the crystallinity is much better, the defects and boundaries will become less, which will improve the photocatalytic activity. Normally, the crystallinity can be improved by calcination in the suitable temperature, which can change the crystal structure and surface area as well [42]. Generally, the specific surface area (as determined by BET measurements) is relevant to the particle size. The smaller particle size and the higher crystallinity of the $NiO/NaTaO_3$:La photocatalyst powder (0.1–0.7 μm) [43] showed the higher efficiency of water splitting into H_2 and O_2 than the nondoped $NaTiO_3$ crystal (2–3 μm), and the reason was that the small particle size with a high crystallinity was advantageous to an increase in the probability of the reaction of photogenerated electrons and holes with water molecules against the recombination. The small particle size to some extent brings about the quantum size effect especially in colloidal system, resulting in widening of a band gap and blue shift in the absorption spectrum, which increases driving force and also leads to a higher activity [26]. In conclusion, optimizing the practical hydrogen or oxygen evolution rate is based on the balance of the various parameters of the architecture.

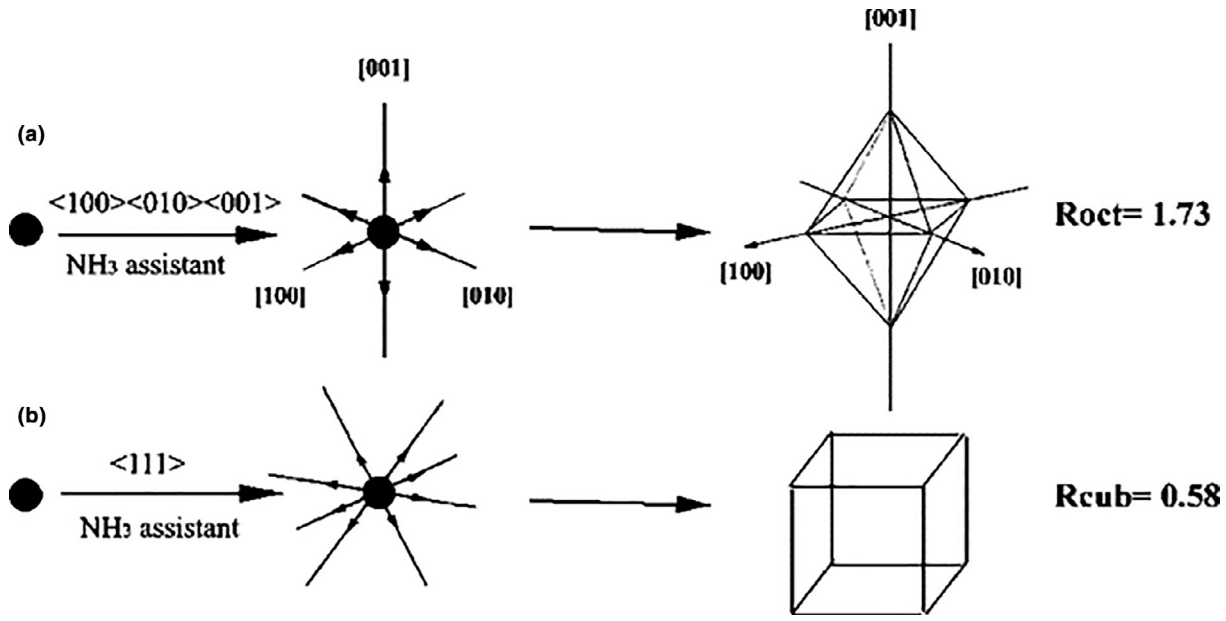

FIGURE 2

Schematic Illustration of the growth mode of Cu_2O (a) octahedra and (b) cubes. The ammonia solution with a certain concentration may favor the preferential crystal growth along the ⟨100⟩ direction and make it far exceed that of ⟨111⟩, thus {100} faces shrink. Reproduced with permission of ([41]). Copyright of 2006 American Chemical Society.

Cocatalysts

The CB levels of many oxide photocatalysts are not negative enough to overcome the overpotential and provide the driving force dynamically for hydrogen evolution. Co-catalysts such as Pt [44], RuO_2 [18], and Ni/NiO [45] usually require a small overpotential and also provide more active sites. At the same time, these cocatalysts can form the Schottky junctions with semiconductors and enhance charge separation in a photocatalyst. Not only water reduction but also the water oxidation can be enhanced by cocatalysts. The most common cocatalysts for oxygen production in the half water oxidation reaction are PtO_x [46,47], IrO_x [48], and CoO_x [49–51]. However, it is not crucial for photocatalytic O_2 evolution to load co-catalysts on oxide photocatalysts because their VBs are usually much more positive than the redox potential of O_2/H_2O (1.23 V *vs.* SHE). But one molecular O_2 is formed by oxidizing water by four holes, which is a more challenging reaction than the 2-electron reduction of H_2O into one molecular H_2 [52], so active sites on cocatalysts for 4-hole oxidation of water are very helpful to enhance the O_2 evolution. For example, in the NiO-loaded $NaTaO_3$ doped with lanthanum system [43], H_2 was produced on the ultrafine NiO particles, while the O_2 evolution proceeded on the groove of $NaTaO_3$:La nanostep structure(Fig. 3), which contributed to the highly efficient water splitting into H_2 and O_2 stoichiometrically. Beside the above-mentioned metals and their oxides acting as cocatalysts, coordination compounds constitute another group of cocatalysts. Such molecular/semiconductor hybrid systems will be described in Section "Advancements in the semiconductor-coordination compound systems for water splitting".

Furthermore, the catalytic performance of cocatalysts can be significantly influenced by their physical and chemical properties, such as particle size and valence states. Usually the more active sites are on the photocatalysts, the better performance the photocatalysts will have. But in most cases, the more active sites induced by cocatalysts would lead to the lowered light absorption of the photocatalysts. Therefore, optimizing the loading amount of the cocatalysts should be considered to obtain the maximum activity of water splitting under light irradiation. Because low-coordinated metal atoms often function as the catalytically active sites, the specific activity per metal atom usually increases with decreasing size of the metal particles. The ultimate small-size for metal particles is the single-atom catalyst (SAC), which contains isolated metal atoms singly dispersed on photocatalysts. SACs maximize the efficiency of metal atom use. Moreover, with well-defined and uniform single-atom dispersion, SACs offer great potential for achieving high activity and selectivity [53–58]. For example, isolated metal atoms (Pt, Pd, Rh, or Ru) stably by anchoring on TiO_2 by a facile one-step method leaded to a 6–13-fold increase in photocatalytic activity over the metal clusters loaded on TiO_2 by the traditional method, as well as enhancing the stability of the photocatalysts [55]. Both measurements and first-principle calculations illustrated that introducing the single-atom Pt could optimize the performance of TiO_2 catalyst in photocatalytic H_2 evolution. Moreover, the catalytic activity of this isolated Pt atom could be even better than that of the metallic Pt deposited on TiO_2, owing to the decreased H^* adsorption energy on Pt and increased exposing reaction sites, which is closer to the optimum thermodynamically [55].

Cocatalysts, by definition, should lower the activation energy of the reaction taking place at their surfaces. In photocatalysis the 'cocatalyst' term is often incorrectly used for any surface decoration which improves the charge separation and therefore decreases the recombination rate, but cannot reduce activation energy. Although such effect is in general desired, it has nothing to do with a real catalytic process.

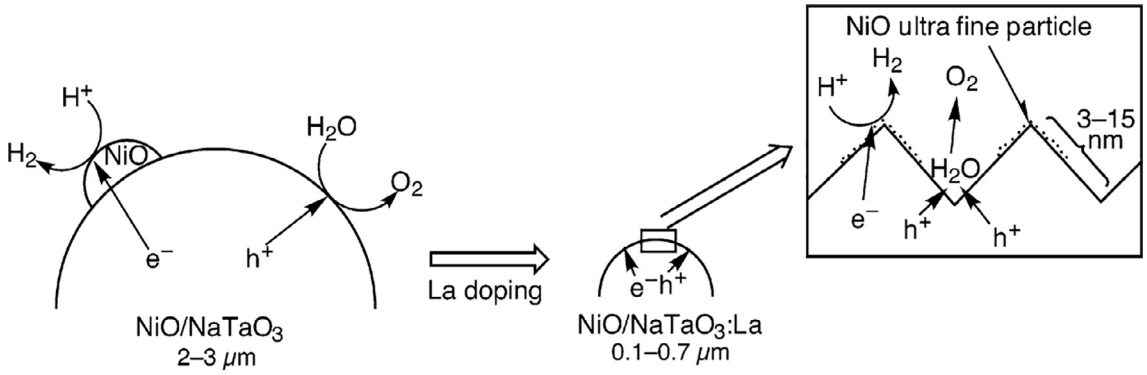

FIGURE 3

Mechanism of highly efficient photocatalytic water splitting over $NiO/NaTaO_3$:La photocatalysts. The small particle size and the ordered surface nanostep structure created by the lanthanum doping contributed to suppression of recombination between photogenerated electrons and holes and the separation of active sites to avoid the back reaction, resulting in the highly efficient water splitting into H_2 and O_2. Reproduced with permission of ([43]). Copyright of 2003 American Chemical Society.

The solution pH

Because the different pH can change the band edge levels, surface chemistry and the states of compounds in a suspension system, the solution pH is one of the key factors influencing the semiconductor photocatalysis, especially in a Z-scheme water splitting system. In 2007, the dependence of the photocatalytic activity of the ($Pt/SrTiO_2$:Rh)–(WO_3)–($FeCl_3$) system on pH under visible light irradiation was studied in the solution containing Fe^{III} ions [59]. The activity of the ($Pt/SrTiO_2$:Rh)–WO_3 Z-scheme system in sulfuric acid solution was increased when pH value changed from 1.3 to 2.4, while decreasing when the pH increased to 2.5. The highest activity was obtained in the aqueous $FeCl_3$–H_2SO_4 solution with pH 2.4. Some other researchers found that a change in the pH of the solution could change the band edge potential [60,61]. It shows that the energy varies in a Nernstian fashion with log (proton activity) over an enormous solution acidity (basicity) range, proved by the CB edge measurements for nanocrystalline TiO_2 [61]. At the same year, the rates of gas evolution over the mixture of Pt–TiO_2–A and bare TiO_2–R (rutile, 2 m^2/g, Toho titanium Co. Ltd. HT0210) suspended in 0.1 M NaI aqueous solutions [62] were observed when increasing the pH value. The rates of both oxygen and hydrogen evolutions significantly increased along with the increasing pH value from 3 to 9. And then it decreased as the solution pH increased to 11. Here, accumulation of I_3^- ions took an important role in the water redox system. At pH from 5 to 7, the amount of O_2 was lower than the stoichiometric ratio to the H_2 amount which facilitated the generation and accumulation of I_3^- in the solution. Therefore, the strong absorption of the I_3^- anions around 350 nm caused a light loss, resulting in a lower efficiency of the photocatalytic reaction. In basic conditions of pH >9, the simultaneous evolution rates of H_2 and O_2, with a stoichiometric ratio (2:1), were much higher than those in acidic conditions. These results illustrate that a basic condition is more favorable for efficient water splitting because the redox cycle of IO_3^-/I^- efficiently takes place.

On the other side, adjusting the suitable pH value could also improvement the stability of the photocatalysts and reactant species. In 2005, the photocatalytic performance of the RuO_2-loaded GaN:ZnO [7] was found to be strongly dependent on the pH value of the aqueous solution. The activity increased as the pH decreased from pH = 7, passing through a maximum at pH = 3, and then decreased. The reason is that (oxy)nitride materials usually have an inherent instability in basic media but are stable in acidic media, resulting in the highest activity at pH = 3.

In electrochemistry, most non-noble-metal hydrogen evolution reaction (HER) electrocatalysts work well only in acidic medium to reduce H_3O^+ [39,63–65]. However, many water-alkali and chloro-alkali HER electrolyzers need alkaline-active catalysts and many microbial electrolysis cells need neutral-active electrocatalysts [39,63,64]. Thus, it is substantially important to adjust the pH value in the reaction and explore out some electrocatalysts satisfying the requirements of the oxidation/reduction potentials and active over a wide pH range (pH = 0–14) at the same time [65–67].

The above studies all indicate that adjusting the proper pH in a suspension system can improve the hydrogen or oxygen evolution rate due to acquiring better reaction environments including the stability of reactants, the concentration of aqueous reagents, the absorption at the certain wavelength and the band edge levels.

Sacrificial and mediator reagents

The half reaction of water reduction into H_2 in particular oxidation into O_2 is very inefficient due to the rapid recombination of the excited holes and electrons on the surface of the photocatalyst. But the more gas production can be achieved by the addition of a suitable sacrificial reagent (a hole or electron scavenger). In principle, the sacrificial reagent tends to react with one type of charge carrier while the other type of carrier reacts with water to produce hydrogen or oxygen. A hole scavenger (an electron donor) can consume generated holes on the surface of the photocatalyst and be used for water reduction half reactions. On the opposite side, an electron scavenger (an electron acceptor) can react with the generated electrons and be needed in the water oxidation reaction. Theoretically, the hole scavengers must have a stronger power to capture photoexcited holes than water due to their less positive potential [68], while the electron scavengers must be more readily reduced than water by

photoexcited electrons. Methanol [69], ethanol [70], ethylenediaminetetraacetic acid (EDTA) [71], triethanolamine (TEA or TEOA) [72], and aqueous solutions of $K_2SO_3 + Na_2S$ [73,74] or $Na_2SO_3 + Na_2S$ [75] are widely acknowledged as good electron donors for the photocatalytic hydrogen evolution, whereas the metal salts such $AgNO_3$ [76], $Na_2S_2O_8$ [77], KIO_3 [78], and $NaIO_3$ [79] are usually used as electron scavengers.

Different from sacrificial agents, mediator shuttles take the necessary roles in the Z-scheme systems or dual systems (Fig. 4). The mediator shuttles usually have two different molecules, so that they can capture the electrons from one semiconductor as well as the holes from another semiconductor. At the same time, these two molecules take the redox reaction, so that they can return to their original chemical states. More importantly, it needs two different photocatalysts, in which one can provide the holes to one mediator molecule and the left excited electrons for H_2 evolution, and the other can provide the excited electrons to recombine with hole mediators and the left excited holes for O_2 evolution in the water splitting system. The most popular mediators are IO_3^-/I^- [47], I_3^-/I^- [46,52] and Fe^{3+}/Fe^{2+} [46,52]. The use of these mediator molecules is, however, not free of some serious drawbacks. For example, the pairs of IO_3^-/I^- require the exchange of six electrons ($IO_3^- + 3H_2O + 6e^- \rightarrow I^- + 6OH^-$) and proceed in neutral or basic media. This process is often a very slow step and requires an effective cocatalyst, such as Pt or PtO_x. Moreover, an unwanted side reaction (competing with water splitting) leading to the I_3^- production takes place at low pH. I_3^- ions absorb efficiently UV and visible light and play the role of a light shield. However, the Fe^{3+}/Fe^{2+} redox pairs appear reversible only at pH lower than 2, since at higher pH precipitation of $Fe(OH)_3$ takes place [80]. Recently, coordination compounds were reported as electron transfer mediators, which will be detailed in Section "Advancements in the semiconductor-coordination compound systems for water splitting".

Nonsacrificial Z-scheme water splitting systems are the eventual goal for the artificial conversion of solar energy into renewable chemical fuels [52]. But this system has some drawbacks compared to the one-step system, such as a higher complexity and double photons are needed for producing the same amount of charges reacted [81]. More vivid examples of Z-scheme water splitting systems will be described in detail in the Section "Z-scheme systems for water splitting".

In summary, according to the main process, there are many properties that influence the photocatalytic reaction of semiconductor photocatalysts in water redox, as mentioned above including bandgap energy, charge separation and migration, lastly charge carriers' reaction at effective sites based on the mechanism as explained in Section "Mechanism". In essence, light absorption could provide pairs of charge carriers [32]. These electron-hole pairs could collapse by recombination or separate, forming independent hole and electrons [83]. Here the recombination rate of these charge carriers competed with their separation and motivation rate. So the key to improve the ability of light absorption is to increase the creation of electron-hole pairs and reduce their recombination, which are affected largely by the composition and nature of the photocatalysts. Doping could induce generation of electron-hole pairs upon irradiation by narrowing the band gap [83] as detailed in Section "Doping", however, the presence of impurities, particle size, surface area and other physicochemical parameters strongly influence the charge recombination and electron-hole trapping as shown in Section "Architecture parameters". Cocatalysts could assist in electron-hole separation and lower the activation energy or overpotential for H_2— or O_2— evolution reaction on the surface of the photocatalysts, and also increase the stability of materials [84], as discussed in Section "Cocatalysts". In the reaction step of producing H_2 and O_2 products, pH could mostly contribute to change the band edge levels, surface chemistry, and the states of compounds in a suspension (Section "The solution pH"), which is vital in a Z-scheme system. Suitable sacrificial reagents capture the electrons and holes in the O_2 and H_2 evolution respectively, which could restrain the recombination of electron-hole pairs in the photocatalysts. Differently, shuttle electron mediators work as the electron transmission medium

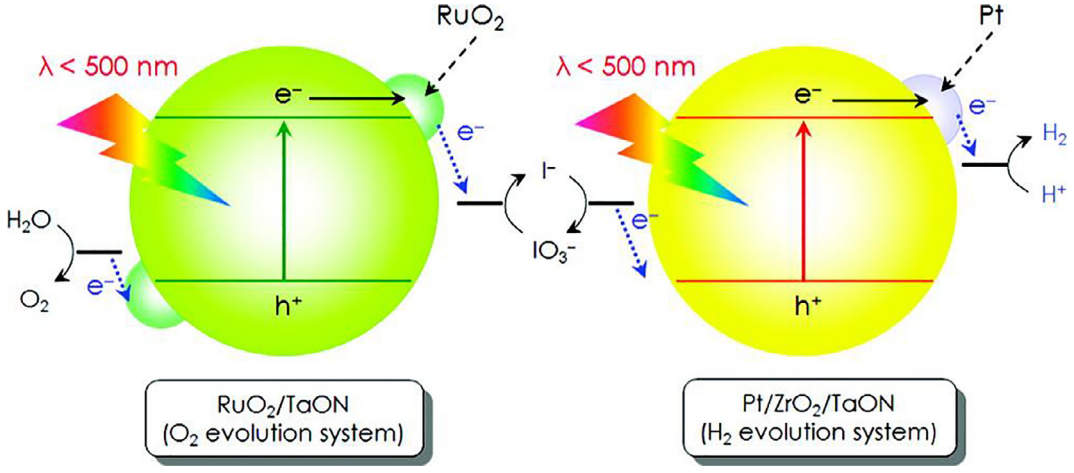

FIGURE 4

Z-scheme system of RuO_2/TaON and Pt–ZrO_2/TaON in aqueous $NaIO_3$ and NaI solution under irradiation. Overall water splitting through two-step photoexcitation was achieved using the optimized RuO_2/TaON photocatalyst in combination with Pt-loaded ZrO_2/TaON as a H_2 evolution photocatalyst from an aqueous NaI solution. Reprinted with permission from ([82]). Copyright (2011) American Chemical Society.

with an acceptor/donor (A/D) pair, suppressing the backward reaction involving redox mediators, facilitating the overall water splitting [85]. Essentially, sacrificial and mediator take the roles of the accepter or/and donor reacting with the photogenerated electrons and holes, which is detailed in Section "Sacrificial and mediator reagents". Overall, these factors should be considered comprehensively in promoting the photocatalytic performance in the overall water splitting system, however, cocatalysts should give priority, as they largely hinder the charge recombination, which is currently the most serious factor in limiting solar to fuel conversion efficiency.

Development of inorganic photocatalysts (oxides, nitrides and sulfides) for visible light-driven water splitting

The developments of photocatalysts working for half reactions are mentioned in Sections "Oxide photocatalysts for half reactions", "(Oxy)nitride photocatalysts" and "(Oxy)sulfide photocatalysts", which can be used as the candidates for the exploration of the novel photocatalysts working in the overall water splitting systems which produce H_2 and O_2 simultaneously under visible light irradiation as illustrated in Sections "The single photocatalyst for overall water splitting" and "Z-scheme systems for water splitting".

Oxide photocatalysts for half reactions

Suitable band positions are required for photocatalysts to produce H_2 or O_2 with sacrificial reagents under visible light irradiation. The bandgaps for native visible light-driven photocatalysts must be narrower than 3.0 eV and the bottom of CB must be more negative than the reduction potential of H^+/H_2, as well as the top of VB more positive than the oxidation potential of O_2/H_2O. As such a dilemma, it is very challenging to find a native photocatalyst for pure water splitting while most of them are only active for half reaction. Metal oxides as water redox photocatalysts are attractive because of their robustness. The typical native and robust visible light-driven oxide photocatalysts, such as WO_3-, $BiVO_4$-, and ABO_3-type photocatalysts, are listed in Table 1 and the corresponding details are illustrated in the following contents.

Firstly, WO_3 is one of the most well-known photocatalysts for O_2 evolution under visible light irradiation in the presence of suitable reagents, considering that the potential of the top of the VB of WO_3 is much higher than the potential of O_2 evolution [86]. Another excellent visible light-driven photocatalyst for O_2 evolution is $BiVO_4$. This is because $BiVO_4$ has a 2.4 eV band gap which is narrower than that of WO_3, and also has the potential of the VB edge at +2.86 V *vs.* RHE, which is deep enough for oxidizing water to produce O_2 theoretically [97]. Practically, $BiVO_4$ as a photocatalyst also needs sacrificial reagents which consume the electrons, beneficial for the separation of the generated electrons and holes in water oxidation reaction. $AgNO_3$ showed the better efficiency than $Fe(NO_3)_3$ as a sacrificial reagent for the water oxidation into O_2 by $BiVO_4$ due to the efficient separation of the photogenerated electron-hole pairs by the Ag ions [89]. Another way to remarkably enhance the photocatalytic activity of $BiVO_4$ is combined with cocatalysts. For example, Pt/MnO_xBiVO_4 [98] got the much high O_2 evolution rate of 650 μmol h^{-1} g^{-1} under visible light ($\lambda \geq 420$ nm), because of

TABLE 1

Oxide, doped oxide, and nanocomposite oxide heterojunction photocatalysts for visible light-driven half water splitting reaction reported over the past few years.

Photocatalysts	BG/eV	Light source	Co-catalyst	Reactant solution	Activity/μmol h^{-1} (0.1 g)		Refs. (Year)
					H_2	O_2	
WO_3	2.8	Hanau Sunset Lamp, λ >410 nm	–	$AgNO_3$	–	0.27	[86] (1983)
$Sr_{0.9}NbO_3$	1.9	Metal halide, $\lambda \geq$420 nm	–	Oxalic acid	4.48	–	[76] (2012)
			–	$AgNO_3$	–	3.5	
IrO_2	1.5	Xe 300 W, λ >400 nm	–	$Na_2S_2O_8$	–	632.4*	[77] (2011)
$KTaO_3$	3.4	Xe 300 W, λ >400 nm	Ag	Methanol	2.59		[87] (2015)
$LaFeO_3$	2.1	W 200 W	Pt	Ethanol	331.5	–	[70] (2012)
$SrTiO_3$	3.2	Xe 300 W, $\lambda \geq$420 nm	Pt	Methanol	18.8	–	[88] (2009)
$BiVO_4$	2.4	Xe 300 W, λ >420 nm	–	$AgNO_3$	–	240	[89] (2008)
$BiVO_4$	2.4	Xe 300 W, $\lambda \geq$420 nm	Pt & Co_3O_4	$NaIO_3$	–	106.9	[79] (2014)
$SrTiO_3$:Rh	2.3	Xe 300 W, λ >300 nm	Pt	Methanol	124	–	[34] (2015)
$SrTiO_3$:La–Cr	2.8	Xe 300 W, λ >420 nm	Pt	Methanol	9	–	[35] (2015)
M-$LaCo_{0.7}Cu_{0.3}O_3$	2.4	Xe 125 W, $\lambda \geq$400 nm	–	Formaldehyde	113	–	[36] (2015)
$Ba_5Ta_4O_{15}$:N	1.8	Xe 300 W, λ >420 nm	–	Methanol	42	–	[90] (2011)
$BaTiO_3$:Rh		Xe 300 W, λ >420 nm	Pt	Methanol	30.8	–	[37] (2014)
$CaIn_2O_4/Fe–TiO_2$	3.4/2.9	Xe 300 W, 420 nm $\leq \lambda \leq$750 nm	–	KI	28	–	[38] (2014)
Carbon quantum dots/TiO_2	–/3.2	Halogen, λ >450 nm	–	Methanol	1.0	–	[91] (2014)
C-mesoporous TiO_2	–	Xe 450 W, $\lambda \geq$400 nm	Pt	Methanol	20	–	[92] (2014)
ZnO/In_2O_3	3.1/2.3	Hg 125 W, $\lambda \geq$400 nm	–	Methanol	178.4	–	[93] (2014)
Bi_2O_3/($BaTaO_3$:Bi)	2.8/3.6	Hg 125 W, $\lambda \geq$400 nm	–	Methanol	102.5	–	[94] (2012)
$Gd_2Ti_2O_7/GdCrO_3$	3.2/2.7	Hg 125 W, $\lambda \geq$400 nm	–	Methanol	1231.5	–	[95] (2011)
$Gd_2Ti_2O_7/In_2O_3$	3.2/2.6	Hg 125 W, $\lambda \geq$400 nm	–	Methanol	579.8	–	[96] (2013)

* O_2 was formed for 3.7 mg IrO_2 nanocrystals at an initial rate of 0.39 μmol/min, and the rate then declines to zero after 3.5 h [77].

not only the intrinsic difference of charge separation between the {0 1 0} and {1 1 0} facets of $BiVO_4$, but also the selective deposition of suitable reduction and oxidation cocatalysts onto the different facets of $BiVO_4$. These heterogeneous water oxidation catalysts can be readily interfaced with electrodes or photosensitizers to achieve effective photocatalytic water oxidation. On the other hand, homogeneous molecular water oxidation catalysts based on a range of transition-metals, such as Ru complexes [99,100], Ir complexes [101,102], Co complexes [103–105], and polyoxometalates [106–112], allow for the further structural fine-tuning and optimization in achieving enhanced catalyst stability, which is pivotal in character ensuring their durability during water oxidation reaction and is introduced in detail in Section "Coordination compounds as molecular cocatalysts".

Visible light-active ABO_3-type photocatalysts also play an important role in the photocatalysis as their perovskite structure is very stable. Uniform crystals and irregular network $LaFeO_3$ [70] was synthesized by a sol–gel method, which evolved large amount of H_2 for ethanol assisted water reduction reaction under visible light illumination. Recently, Ag-decorated $KTaO_3$ and $NaTaO_3$ nanotubes were directly monitored [87] to improve water redox performance under simulated sunlight and visible light. Due to the high photocatalytic performance, economic cost, and excellent stability, $SrTiO_3$ has been one of the most attractive photocatalysts for water reduction as well. Mesoporous-assembled $SrTiO_3$ [88] was synthesized by the sol–gel method with the aid of a structure-directing surfactant, which had a better photocatalytic activity with hydrogen production rates of 188 $\mu mol\ h^{-1}\ g^{-1}$ and the solar to hydrogen energy (STH) conversion of 0.9% under visible light irradiation than commercial $SrTiO_3$ and commercial TiO_2 (P-25).

For the photocatalysts inactive under visible light irradiation, doping with suitable elements or composing with other photocatalysts can realize their photocatalytic activities in the visible light region as shown in the middle part of Table 1. Rhodium is one of the most common doping elements. A few p-type semiconductors have been researched by doping rhodium, for example $SrTiO_3$ [34] and $BaTiO_3$ [37], which got more negative VB potentials, forming new absorption bandgaps in visible light region to promote the water reduction ability. Copper is another frequently used doping element owing to its universality and non-toxicity. Doping copper in the perovskite photocatalyst $LaCoO_3$ [36] could create the appropriate oxygen vacancy, leading to more negative VB, than excellent visible light-driven photocatalytic activity of hydrogen evolution (1130 $\mu mol\ h^{-1}\ g^{-1}$). Numerous non-metallic anionic dopants have been widely used in $BiVO_4$ replacing V^{5+} to enhance the n-type characteristics and then showed the better photocatalytic performance, such as carbon [113] and phosphate [114]. One step fabrication of C-doped $BiVO_4$ with hierarchical structures significantly improved the absorption enhancement under visible light and the efficient separation and transfer of the photogenerated electrons and holes, with the best photocatalytic activity (ca. 800 $\mu mol\ L^{-1}$, after 5 h) in O_2 evolution from water under visible light irradiation ($\lambda \geq 420$ nm) [113]. Transition metal doping usually forms a discrete level in the forbidden band of photocatalyst and reduces the mobility of electrons and holes in the dopant level and thus sometimes lowered activity, however, the photocatalytic activity of $BiVO_4$ for water oxidation was found to be remarkably enhanced by 2 atom% molybdenum doping, resulting into 370 $\mu mol\ h^{-1}\ (0.5\ g)^{-1}$ O_2 evolution rate [115]. There are some elements reported rarely, such as La and Cr [35], which were doped into $SrTiO_3$ by a one-pot microwave-assisted method and improved the photocatalytic hydrogen production performance by 15 times under visible light irradiation than La doped $SrTiO_3$.

Different from doping, composite nanostructures do not change the band positions of the oxide semiconductors but increase visible absorption by a narrow band semiconductor and mitigate charge recombination by junction structure, consequently optimizing the water reduction or oxidation reaction. The end part of Table 1 summarizes the photocatalytic activity of typical nanocomposite oxide heterojunctions. Several oxide photocatalysts, including TiO_2, In_2O_3, and perovskite-type oxides, were studied as components of composites with other photocatalysts. The first and the most common photocatalyst, P25 TiO_2, was combined with carbon quantum dots [91] by a one-step hydrothermal reaction, which improved the photocatalytic H_2 production activity under UV–vis and visible light (λ >450 nm) without any additional metal cocatalyst. When CQDs/P25 was irradiated by the UV light, the electrons and holes were mainly excited on TiO_2 and then the excited electrons moved to the CQDs as the electron acceptors, which benefits charge separation. However, under the visible light illumination, the charge pairs were also excited on the π-conjugated CQDs and then CQDs acted as a photosensitizer to transfer the electrons to P25, accelerating the visible light-driven photocatalytic H_2 production (0.5 $\mu mol\ h^{-1}\ (0.05\ g)^{-1}$) with methanol as a hole scavenger. Similarly, brown carbonate-doped TiO_2 microspheres, synthesized by a simple "one-pot" solvothermal method, could produce 0.2 $mmol\ h^{-1}\ g^{-1}$ H_2, higher than those from various other TiO_2 photocatalysts [92]. In_2O_3 is sensitive to visible light radiation, but its activity is very low. There are many studies combining the single-phase In_2O_3 with other semiconductors to promote their photocatalytic H_2 evolution under visible light irradiation. Loading ZnO on In_2O_3 has successfully improved the photocatalytic water reduction for hydrogen production (1784 $\mu mol\ h^{-1}\ g^{-1}$) under visible light irradiation [93]. Perovskite-type oxide composites, like $Gd_2Ti_2O_7/GdCrO_3$ [95], combined as p–n junction and reduced the possibility of recombination of photogenerated electrons and holes, leading to the highest activity toward H_2 evolution (246.3 $\mu mol\ h^{-1}$ $(0.02\ g)^{-1}$) with apparent quantum efficiency of 4.1% among other photocatalysts.

Usually, the sensitization mechanism is applied to solar cell [124–128]. They have recently been used in visible light-driven photocatalytic H_2 evolution [71,72,116–123], as shown in Table 2. The essence of sensitization is that electron/hole pairs are generated by visible light irradiation in dyes or sensitizers and then electrons are transferred to the CB of a semiconductor. Alternatively, holes are transferred to the VB of a semiconductor. Such mechanisms of photosensitization are often observed mainly in the case of n-type semiconductors [117]. A typical model of transfer of photogenerated electron/hole pairs in sensitized semiconductor is shown in Fig. 5. The sensitizers of TiO_2 have developed rapidly, including Ru(II) complex [118], Eosin

TABLE 2

Sensitized photocatalysts for H_2 evolution in the aqueous suspension under visible light irradiation.

Photocatalyst	Sensitizer	Sacrificial reagent	Light source	H_2 μmol h^{-1} (0.1 g)	Refs. (Year)
Pt–$HCa_2Nb_3O_{10}$	Ru–CH_3	EDTA	Xe-300 W, λ = 420 nm	248	[71] (2015)
Pt–(TiO_2:N)	Eosin Y	TEOA	Hg-400 W, λ >420 nm	80	[116] (2008)
Pt–TiO_2	CdS	Lactic acid	Xe-300 W, λ >420 nm	662.5	[117] (2011)
Pt–Al_2O_3/TiO_2	$[Ru^{II}(4,4\text{-}(CO_2H)_2bpy)_3]^{2+}$	EDTA	Xe-300 W, λ >420 nm	129.3	[118] (2009)
Pt–NS–$H_4Nb_6O_{17}$	$[Ru(bpy)_2(4,4'\text{-}(PO_3H_2)_2bpy)]^{2+}$	EDTA	Xe-300 W, λ >420 nm	288	[119] (2009)
Pt–TiO_2	$[Sn^{IV}(OH_2)_2TPy^HP]^{6+}$	EDTA	Xe-300 W, λ >420 nm	222.2	[120] (2010)
2-Mecaptoethanol/$Ni(Ac)_2$	Erythrosin B	TEOA	Xe-300 W, λ >420 nm	204	[72] (2011)
$K_2La_2Ti_3O_{10}$	CdS	Na_2S	Xe-500 W, λ >400 nm	2.0	[121] (2013)
Pt–TiO_2	Zinc–phthalocyanine	EDTA	Xe-300 W, λ >420 nm	378.2	[122] (2013)
$K_2Ti_4O_9$	PbS	Na_2S–Na_2SO_3–KOH	Xe-300 W, λ >400 nm	61.1	[123] (2012)

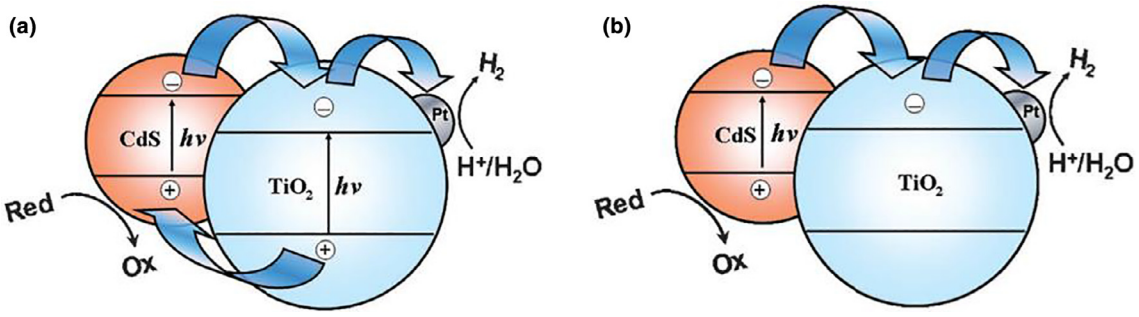

FIGURE 5

Transfer of photogenerated electron/hole pairs in CdS-sensitized TiO_2 under UV (A) and visible light (B) irradiation. Reproduced from ([117]) with permission of The Royal Society of Chemistry (RSC) on behalf of the European Society for Photobiology, the European Photochemistry Association and the RSC.

Y [116], CdS [117], Sn(IV) complex [120] and asymmetric zinc phthalocyanine derivatives [122]. Other common sensitizers are sulfides, such as CdS [117,121] and PdS [123]. Erythrosine B-sensitized Ni(II) salt and 2-mecaptoethanol complex [72] was created and obtained the outstanding photocatalytic efficiencies for hydrogen evolution (2040 μmol h^{-1} g^{-1}) under visible light. Authors claimed it was a simple and environmentally benign solar hydrogen production systems assembled from Ni(II) salt and low-cost xanthene dyes.

Above all, a large amount of oxide photocatalysts have been studied to promote the photocatalytic activity under visible light irradiation. However, the drawback of such oxide photocatalysts still exist which is the large bandgap due to very positive valence band. Doping elements, composing junctions with other photocatalysts or combining with dyes or sensitizers can mediate this problem, which is a direction for modification of robust oxide photocatalysts.

(Oxy)nitride photocatalysts

(Oxy)nitrides have become potential photocatalysts for water splitting under visible light irradiation due to their narrow band gap when nitrogen atoms replace oxygen atoms in the crystal structure. Many (oxy)nitrides [25,49–51,129,131,132] have been explored for hydrogen or oxygen evolution under visible light irradiation in the presence of appropriate reagents as demonstrated in Table 3. Among various (oxy)nitrides, tantalum nitride (Ta_3N_5) [51] could absorb visible light (λ <590 nm) to generate electrons and holes for water oxidation into oxygen with an

TABLE 3

(Oxy)nitride photocatalysts for water redox into H_2 or O_2 under visible light irradiation.

Photocatalyst	BG/eV	H_2 evolution		O_2 evolution		Refs. (Year)
		Cocatal.	Activity/μmol h^{-1}	Cocatal.	Activity/μmol h^{-1}	
$LaTiO_2N$	2.1	–	–	CoO_x	204	[49] (2015)
Na_2CO_3/Ta_3N_5	2.1	–	–	CoO_x	450	[51] (2012)
$BaNbO_2N$	1.7	Pt	0.04	CoO_x	60	[50] (2013)
$CaTaO_2N$	2.5	Pt	8.3	–	–	[129] (2012)
$SrNbO_2N$	2.1	Pt	9.3	–	0.5	[130] (2005)
m-ZrO_2/TaON	2.4	Pt	6	–	0.20	[131] (2008)
$BaTaO_2N$	1.8	Pt	2	CoO_x	10	[132] (2015)
$CsCa_2Ta_3O_{9.7}N_{0.2}$	2.1	Rh	0.47	–	9.2	[133] (2012)
$Y_2Ta_2O_5N_2$	2.2	Pt–Ru	250	–	140	[25] (2004)

evolution rate of 450 μmol h^{-1} (0.1 g)$^{-1}$, thus a promising nitride semiconductor for visible light-driven water oxidation. The bulk-type compounds with a perovskite-like structure, like tantalum oxynitrides [25,129,131–133], titanium oxynitrides [49] and Nb-based perovskite-type oxynitrides [50], also successfully extended the absorption region to visible light for photocatalytic water splitting into hydrogen or oxygen. Especially, $Y_2Ta_2O_5N_2$ catalyst was synthesized by nitriding $YTaO_4$ under ammonia flow, resulting in a small optical bandgap energy of 2.2 eV [25]. The activity of H_2 evolution was increased by co-depositing both Pt and Ru on the $Y_2Ta_2O_5N_2$ catalyst, up to a maximum of 833 μmol h^{-1} g^{-1} with 0.15 wt% Pt and 0.25% Ru. The rate was 22 times larger than that for 0.15 wt% Pt/$Y_2Ta_2O_5N_2$. Upon irradiation, O_2 was produced at an initial rate of 140 μmol h^{-1} (0.3 g)$^{-1}$ from 0.01 M $AgNO_3$ solution over $Y_2Ta_2O_5N_2$. A tantalum oxynitride series $ATaO_2N$ (A = Ca, Sr, and Ba) and $PrTaON_2$ were prepared by growth methods and their VB and CB edges could vary systematically [134]. The CB edges of tantalum oxynitride perovskite could be tuned by modifying the size of the A-site cation. Smaller A-site cations brought to more octahedral titling and less disperse CBs and thus a higher energy for the CB edge. The VB edges could be changed by adjusting the oxygen-to-nitrogen ratio. An upward shift in the position of VB edge was leaded by increasing the nitrogen content. This study could determine the absolute energy levels of the oxynitride band edges, exploiting their intrinsic potential as photocatalysts.

The most common challenging for the (oxy)nitride photocatalyst is to prepare high-quality (oxy)nitrides to reduce the defect density in surface layers, as the formation of defects seems inevitable especially near the surface in the conventional preparation method of transition metal (oxy)nitrides using NH_3. The radicals formed by the decomposition of NH_3 between the interior and exterior of the statically placed lump of oxide powders could be different. The degree of nitridation and the homogeneity of each particle in a powder sample could be very low. So it is very important to dope the entire sample with nitrogen as homogeneously as possible by repeating nitridation with grinding and mixing the nitrogen precursor a few times and to ensure as uniform NH_3 flow as possible by reducing a single nitrided amount of precursor [135]. High-pressure high-temperature treatments [136], acid treatments [137] and flux treatments [138,139] could also be utilized in the syntheses and post-treatments on (oxy)nitride photocatalysts to enhance the crystallinity and reduce the impurities, finally improving their photocatalytic performance.

Above all, (oxy)nitrides can generate both H_2 and O_2 individually from H_2O in the presence of suitable sacrificial agents under visible light irradiation, as the narrowed bandgaps have been achieved by nitrogen atoms replacing oxygen atoms in the crystal structure and upward shifting the position of VB edge. The main challenge deep-rooted in the thermal instability of (oxy)nitrides compared to the corresponding oxides is to reduce the defect density, improve the crystallinity and inhibit decomposition by various post-treatments.

(Oxy)sulfide photocatalysts

In the metal oxide photocatalysts, the tops of VBs are always located at very positive potentials, close to +3 V *vs.* RHE due to the O 2p orbitals, while the bottoms of CBs of some transition metal oxides are localized at potentials more negative than 0 V *vs.* RHE because of their empty d orbitals, resulting in very wide energy band gaps. S 3p orbital is more negative than O 2p, so sulfides always show a narrow bandgap due to the raised VB composed of S 3p.

As such many sulfides were reported as visible light-driven photocatalysts. Table 4 lists the (oxy)sulfides reported for the H_2 evolution with suitable reagent. Among them, CdS has a narrow band gap of 2.4 eV, therefore having been widely studied. Loading Ni [142] on CdS could significantly enhance the H_2 production under visible light in the appropriate reagent, where a maximum hydrogen production rate of 25.848 mmol h^{-1} g^{-1} was acquired at 4% dosage of Ni dopants. 0.2 wt% MoS_2 [147] loaded on CdS could also increase the activity of the H_2 evolution up to 36 times than that of pure CdS, and even had better photocatalytic performance than that of 0.2 wt% Pt/CdS under the same reaction conditions. As a rare H_2 evolution photocatalyst, MoS_2 was prepared as colloidal nanoparticles to catalyze water into H_2 in $[Ru(bpy)_3]^{2+}$-based molecular systems under visible light [146]. ZnS, although it has a wide band gap of 3.6 eV, is also a popular photocatalyst for visible light-driven water reduction when combined with other ingredients. For example, $Cd_{0.5}Zn_{0.5}S$ combining the advantage of CdS and ZnS was prepared by a simple hydrothermal method and markedly enhanced the photocatalytic activity of hydrogen production when doping with Bi^{3+} [143]. Ni atoms exchanging a quite few percent of Zn atoms in ZnS could narrow the energy band into 2.3 eV and increased the hydrogen amount in the photocatalytic water reduction under visible light [24]. ZnS was also combined with a narrow band gap photocatalyst, such as $AgInS_2$ [74] or $CuLnS_2$ [73] to create a new solid solution. For instance, Pt (3%)-loaded $(AgIn)_{0.22}Zn_{1.56}S_2$ solid solution [74] showed a very high activity of H_2 evolution up to 3147 μmol h^{-1} g^{-1} in visible region and a quantum yield of 20% at 420 nm. ZnS–$CuInS_2$–$AgInS_2$ solid solution photocatalysts were also investigated for the water reduction to H_2 evolution under visible light irradiation. The system showed a better photocatalytic performance (7733 μmol h^{-1} g^{-1}) when Ru was loaded on this solid solution as a cocatalyst [73]. The highest activity of H_2 generation by sulfides photocatalyst reported so far is 8.77 mmol h^{-1} (0.3 g)$^{-1}$ and the corresponding QE is extremely high up to 93%, achieved by loading as low as 0.30 wt% of Pt and 0.13 wt% of PdS as cocatalysts on CdS [153].

Various metal sulfides were also deposited on $CuGa_3S_5$ as shown in Table 5, and found that NiS— and FeS had a better performance than other cocatalysts [141]. In_2S_3 [145] was also used to decorate TiO_2 nanoparticles, which achieved the hydrogen production of 1350 μmol h^{-1} g^{-1} under visible light (λ >420 nm) irradiation due to narrow bandgap of In_2S_3 and its catalytic effect. $AgIn_5S_8/TiO_2$ heterojunction nanocomposite [144] and CdS/$AgGaS_2$ p–n-type photocatalytic diodes [75] were also prepared to promote the hydrogen production (850 and 3000 μmol h^{-1} g^{-1}, respectively) under visible light. As the AB_2X_4-type semiconductor has a layered structure, $ZnIn_2S_4$ was optimized by copper doping, which increased the hydrogen evolution from 26.1 to 151.5 μmol h^{-1} (0.2 g)$^{-1}$ in the aqueous solution of Na_2SO_3 and Na_2S [140]. $Sm_2Ti_2S_2O_5$ with the layers of S—(TiO_2)—O—(TiO_2)—S (double octahedral) [148] was very stable for producing

TABLE 4

(Oxy)sulfide photocatalysts for water splitting into H_2 under visible light irradiation.

Photocatalyst	BG/eV	Light source	Reagent	H_2 evolution		Ref. (Year)
				Activity/μmol h^{-1}	QY (%)	
$ZnIn_2S_4$:Cu	2.1	Xe-300 W, >430 nm	Na_2SO_3 + Na_2S	151.5 (0.2 g)	14.2 (420 nm)	[140] (2008)
$CuGa_3S_5$: NiS	2.4	Xe-300 W, >420 nm	Na_2SO_3 + Na_2S	49 (0.05 g)	1.3 (420–520 nm)	[141] (2010)
Pt–CdS/$AgGaS_2$	2.4/2.7	Hg-450 W, >420 nm	Na_2SO_3 + Na_2S	473 (0.1 g)	19.7 (420 nm)	[75] (2007)
Ni–CdS	2.4	Xe-300 W, >420 nm	$(NH_4)_2SO_3$	25.8 (0.1 g)	26.8 (420 nm)	[142] (2015)
$Zn_{0.999}Ni_{0.001}S$	2.3	Xe-300 W, >420 nm	K_2SO_3 + Na_2S	280 (1g)	1.3 (440 nm)	[24] (2000)
Pt–$Cd_{0.5}Zn_{0.5}S$:Bi	2.3	Hg-400 W, >420 nm	Na_2SO_3 + Na_2S	55.9 (0.1 g)	9.7 (400–700 nm)	[143] (2012)
Ru–$(CuAg)_{0.15}In_{0.3}Zn_{1.4}S_2$	1.9	Xe-300 W, >420 nm	K_2SO_3 + Na_2S	2320 (0.3 g)	–	[73] (2006)
$AgIn_5S_8/TiO_2$	1.8/	Xe-300 W, >420 nm	Na_2SO_3 + Na_2S	8.5 (0.1 g)	–	[144] (2013)
In_2S_3/(Pt–TiO_2)	2.3/	Xe-300 W, >420 nm	Na_2SO_3 + Na_2S	135 (0.1 g)	1 (420 nm)	[145] (2011)
Pt–$(AgIn)_{0.22}Zn_{1.56}S_2$	2.3	Xe-300 W, >420 nm	K_2SO_3 + Na_2S	944 (0.3 g)	20 (420 nm)	[74] (2004)
Ru$(bpy)_3^{2+}$/MoS_2/H_2A	–	Xe-300 W, >420 nm	Acetonitrile + Methanol	83.3 (0.002 g)	–	[146] (2009)
MoS_2–CdS	2.4	Xe-300 W, >420 nm	Lactic	540 (0.1 g)	–	[147] (2008)
Pt–$Sm_2Ti_2S_2O_5$	2.1	Xe-300 W, >440 nm	Na_2SO_3 + Na_2S	–	0.1	[148] (2002)
Rh/Ag–$Sm_2Ti_2S_2O_5$		Hg-450 W, >400 nm	Na_2SO_3 + Na_2S	949(0.2 g)	8.8 (440 nm)	[149] (2010)
Pt–$La_5Ti_2AgS_5O_7$	1.5	Xe-300 W, >420 nm	Na_2SO_3 + Na_2S	225(0.2 g)	1.2 (420 nm)	[150] (2012)
Pt–La_3GaS_5O	2.3	Xe-300 W, >420 nm	Na_2SO_3 + Na_2S	108	2.5 (420 < λ < 540 nm)	[151] (2008)
Pt–$LaInS_2O$	2.6	Xe-300 W, >420 nm	Na_2SO_3 + Na_2S	9(0.1 g)	0.2 (420 nm)	[152] (2017)
Pt–PdS/CdS	1.6/2.3	Xe-300 W, >420 nm	Na_2SO_3 + Na_2S	8700 (0.3 g)	93 (420 nm)	[153] (2009)

TABLE 5

Rates of H_2 evolution in the presence of 0.05 g $CuGa_3S_5$ loaded with various cocatalysts from an aqueous Na_2S (10 mM) and Na_2SO_3 (10 mM) solution under visible light (λ > 420 nm) irradiation [141].

Entry	Cocatalyst	Rate of H_2 evolution/μmol h^{-1}
1	None	15
2	NiS	49
3	FeS	38
4	Ru_2S_3	29
5	Ag_2S	26
6	CoS	23
7	PdS	21
8	CuS	13

H_2 or O_2 from aqueous solutions with a sacrificial electron donor (Na_2S, Na_2SO_3 or methanol) or acceptor (Ag^+) under visible light (λ <650 nm). Further study found that Ag2S/Rh-modified $Sm_2Ti_2S_2O_5$ had a photocatalytic water reduction activity 9 times that of the $Sm_2Ti_2S_2O_5$ sample and the apparent quantum efficiency of the optimized sample was measured to be ca. 8.8% at 440 nm [149]. Moreover, $La_5Ti_2MS_5O_7$ (M = Ag, Cu) was loaded with Pt for H_2 evolution was significantly high among existing Ti-based oxysulfide photocatalyts with AQE of 1.2% at 420 nm [150]. Simultaneously, $La_5Ti_2MS_5O_7$ loaded with IrO_2 were active for photocatalytic O_2 evolution although the valence band maximum was composed of S 3p orbitals [150].

In total, the best sulfide photocatalyst for H_2 evolution is Ru—$(CuAg)_{0.15}In_{0.3}Zn_{1.4}S_2$ with a H_2 evolution rate of 7733 μmol h^{-1} g^{-1} [153], whereas the sulfide photocatalysts are usually not stable for oxidizing water into O_2 because the S^{2-} anions are more vulnerable to be oxidized than water. Therefore, a sulfur-containing hole scavenger (e.g., Na_2S, Na_2SO_3) is always added to stabilize sulfide-based photocatalysts. In addition, there is no sulfide reported for oxygen production even in the presence of electron scavengers, which is again due to the completion between sulfur ions oxidation and water oxidation. To make sulfides stable, one possible strategy is to make a p-type junction to enable holes transfer to another semiconductor instead of oxidizing itself.

In conclusion, Fig. 6 illustrates the representative oxides, nitrides, and sulfides applied in the visible light-driven water oxidation and reduction. It shows the bandgaps and the VB and CB positions of the selected oxides, nitrides, and sulfide semiconductor photocatalysts, which are appropriate for hydrogen or/and oxygen generation. TiO_2 and ZnO are the most employed photocatalysts [91–93], but their wide bandgaps lead to them being inefficient under visible light irradiation. In order to increase the activity of these photocatalysts and improve their energy conversion efficiency under visible light irradiation, co-catalysts loaded on them or bandgap tuning by doping are widely applied. Very obviously, (oxy)nitrides and (oxy)sulfides usually have narrower bandgap than oxides, due to that the electronic potential of the N 2p or S 3p orbitals are higher than that of than O 2p and the N 2p or S 3p orbitals will dominate the occupancy of the top of the valence band, leading to band-gap narrowing [154]. However, S^{2-} in the mental sulfide photocata-

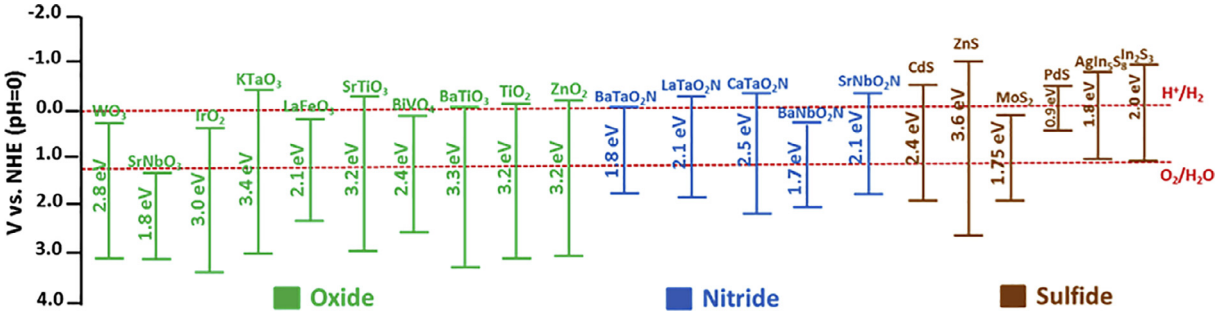

FIGURE 6

Bandgaps and band-edge positions of representative oxide (green), nitride (blue) and sulfide (brown) semiconductors in relation to the redox potentials for water splitting at pH = 0. Values were taken from references given in Tables 1, 3 and 4. The CB potential of a semiconductor material in aqueous solution usually exhibits a pH dependence described according to $E_{CB} = E^{0}_{CB\ (pH\ 0)} - 0.059$ pH. The redox potentials of water also have the same linear pH dependence with a slope of 0.059 V per pH.

TABLE 6

Single photocatalyst for water splitting under visible light irradiation.

Photocatalyst	Cocatalyst	Activity/μmol h^{-1}		QY (%)	Ref. (Year)
		H_2	O_2		
$In_{0.85}Ni_{0.10}TaO_4$	NiO_x	16.6	8.3	0.66(402 nm)	[45] (2001)
$(Ca_{1-x}Zn_x)N_{1-x}O_x$	Ru–Cr oxides	308.6	154.3	2.5(420–440 nm)	[155] (2006)
GaN:ZnO	$Ru_{2-y}Cr_yO_3$	4.6	2.3	0.16(400–500 nm)	[156] (2012)
$Ag_3PW_{12}O_{40}$	CQDs–Ag	4.02	2.01	4.9(480 nm)	[157] (2014)
ZrO_2/TaON	RuO_x/Cr_2O_3–IrO_2	3.8	1.9	<0.1(420 nm)	[158] (2013)
$(Zn_{1.44}Ge)(N_{2.08}O_{0.38})$	RuO_2	14.2	7.4	–	[159] (2007)
Cu_2O	–	2	1	0.3(550–600 nm)	[160] (1998)
GaN:ZnO	Mn_3O_4–Rh/Cr_2O_3	11.7	5	1	[161] (2000)
N-doped graphene oxide–quantum dots	–	0.45	0.25	–	[162] (2014)
CdS	Carbon dots	0.13	0.06	–	[163] (2017)
CoO	Carbon dots	1.67	0.91	1.02(420 nm)	[164] (2017)
Te/SnS_2 ANLs	Ag	332.4	166.2	–	[165] (2017)

lysts is preferably oxidized by photogenerated holes accompanied with creation of sulfur [26], whereas, CdS is an excellent photocatalyst for H_2 evolution under visible light irradiation, if an efficient hole scavenger exists. The (oxy)nitrides have similar drawback to the sulfide, although the former is a bit more stable than the latter under light irradiation. Meanwhile, WO_3 has a good photocatalytic performance for water oxidation into O_2 under visible light irradiation in the presence of an electron acceptor such as Ag^+ and Fe^{3+} but is not active for H_2 evolution because of its low conduction band level. Some of oxynitirdes, e.g., $LaTiO_2N$, $BaNbO_2N$, and $Y_2Ta_2O_5N_2$, can also photo-oxidize water to oxygen while sulfides cannot. The band gap of a visible light-driven photocatalyst should be narrower than 3.0 eV. $KTaO_3$, $SrTiO_2$, TiO_2, ZnO_2, $LaTaO_2N$, $CaTaO_2N$, and $SrNbO_2N$ possess suitable band structures for overall water splitting as shown in Fig. 6 while their efficiency is rather moderate. Nevertheless, the band structure is just a thermodynamic requirement but not a sufficient condition. Therefore, suitable band engineering and co-catalyst modification are necessary for the design of efficient photocatalysts with visible light response for overall water splitting in Sections "The single photocatalyst for overall water splitting" and "Z-scheme systems for water splitting".

The single photocatalyst for overall water splitting

Photocatalytic water-splitting into H_2 and O_2 based on a single photocatalyst under visible light is a very challenging way to produce renewable energy resource [166] (Table 6). The most simple photocatalyst for the overall water splitting under visible light irradiation was Cu_2O [160], which successfully decomposed water into H_2 and O_2 under visible light irradiation without any additives in the distilled water. However, a part of photocatalysis is not driven by light but mechanical reason [160]. Another simple compound for water splitting under visible light irradiation is nitrogen-doped graphene oxide quantum dots [162], which consisted of the p- and n-type domains, taking responsibility for

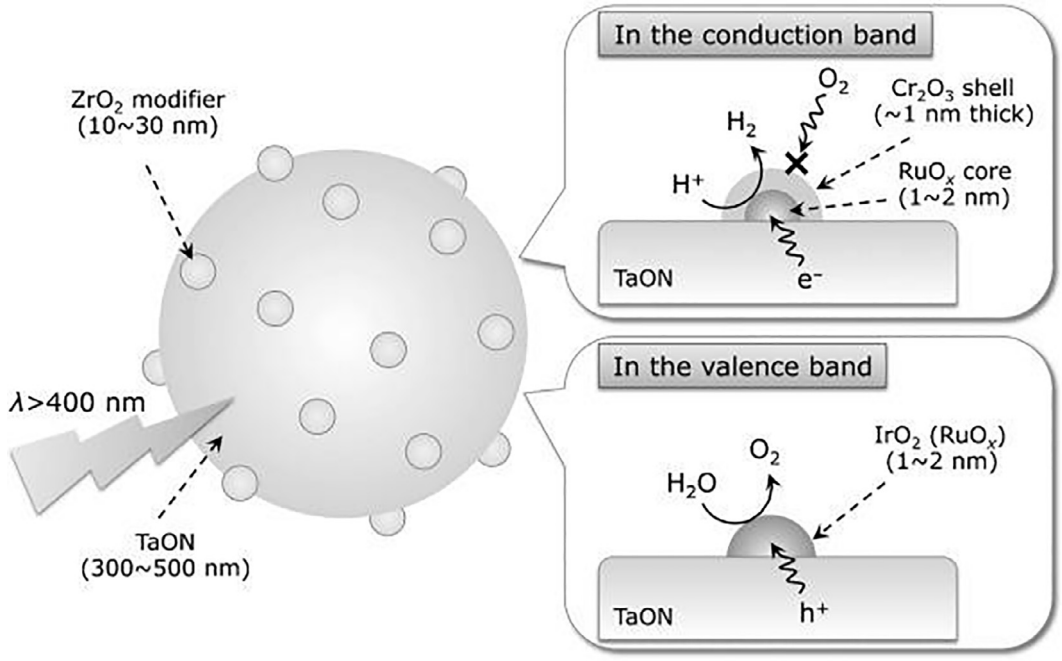

FIGURE 7

Schematic illustration of the mechanism of overall water splitting on $IrO_2/Cr_2O_3/RuO_x/ZrO_2$/TaON photocatalyst. IrO_2 on TaON was demonstrated to function as a water oxidation site, and Cr_2O_3 – coated RuO_2 prevented the water oxidation reaction on RuO_2/TaON but functioned as a water reduction site. Reprinted with permission from([158]). Copyright (2013) American Chemical Society.

electron injection to produce H_2 and hole injection to produce O_2 respectively. Interestingly, carbon dots concentration in carbon dots-CdS nanocomposites could adjust the stoichiometric ratio of generated H_2 and O_2 and Carbon dots could work as both oxidation and reduction sites when the carbon dots concentration is high enough [163]. Similarly, carbon dots (CDs) anchored on the surface of octahedral CoO achieved highly efficient and long-term stable photocatalytic performance for overall water splitting under visible light, showing a H_2 (O_2) evolution rate of 1.67 μmol h^{-1} (0.91 μmol h^{-1}) with an expected 2:1 stoichiometry, which is up to 6 times as high as that of pristine CoO [164]. Carbon quantum dots and silver nanoparticles were also decorated on the polyoxometalate ($Ag_3PW_{12}O_{40}$) as cocatalysts for water splitting into H_2 and O_2 efficiently under visible light [157]. In this system, $Ag_3PW_{12}O_{40}$ took the main role for water splitting. CQDs could prevent the dissolution of the photocatalysts in aqueous solution and also could store electrons to decrease the electron-hole recombination rate on the surface of the photocatalyst. Ag nanoparticles played two vital roles: one was to capture the electrons from the CB and CQDs, acting as catalytic sits for hydrogen generation, the other was to generate electrons due to its strong localized surface plasmon resonance (LSPR) near the $Ag/Ag_3PW_{12}O_{40}$ interfaces. Similarly, Ag nanoparticles decorated on surface of SnS_2 nanoplates (n-type) served as excellent electron collector and sources of localized surface plasmon resonance sources, and Te nanowire, a p-type semiconductor served as the branch of $Te/SnS_2/Ag$ artificial nanoleaves (ANLs), which made a "highway" of "Te nanowire-SnS_2 nanoplates-Ag nanoparticles" for efficient light utilization and charge separation, therefore enabled and improved visible light-driven overall water splitting without any sacrificial reagent [165].

Oxynitrides have been widely applied for visible light-driven water splitting as well. ZrO_2/TaON solid solution [158] was modified with suitable cocatalysts for visible light-driven water splitting into H_2 and O_2 without sacrificial reagents as shown in Fig. 7. IrO_2 on ZrO_2/TaON worked as a water oxidation site, while Cr_2O_3/RuO_x provided the water reduction site and the Cr_2O_3 shell prevented water oxidation on RuO_x core. Another solid solution GaN/ZnO was loaded with MnO_3 as a hole acceptor for oxidation reaction to produce O_2 and Rh/Cr_2O_3 as an electron acceptor for reduction reaction to produce H_2, improving water-splitting activity under visible light [161]. Furthermore, loaded one co-catalyst $Rh_{2-y}Cr_yO_3$ on GaN/ZnO realized a long-time overall water splitting with an apparent quantum yield of ca. 0.16% at 400–500 nm [156]. GeO_2 and ZnO were also mixed with each other under ammonia flow to create a wurtzite-type structure $(Zn_{1.44}Ge)(N_{2.08}O_{0.38})$, which was modified by RuO_2 nanoparticles to achieve the overall water splitting under both ultraviolet and visible irradiation [159]. Another solid solution of gallium and zinc nitrogen oxide $(Ga_{1-x}Zn_x)(N_{1-x}O_x)$ was modified with a mixed oxide of rhodium and chromium to produce H_2 and O_2 (462.9 and 105.7 μmol h^{-1} g^{-1}, respectively) efficiently under solar light irradiation and performed 2.5% quantum efficiency at 420–440 nm [155].

$In_{1-x}Ni_xTaO_4$ (x = 0–0.2) was created by doping nickel into indium–tantalum-oxide and split water into hydrogen and oxygen stoichiometrically (33.2 and 16.6 μmol h^{-1} g^{-1}, respectively) under visible light irradiation with a quantum yield of about 0.66% (at 402 nm), which gave an example of more efficient photocatalysts for water splitting by improving its surface area and suitable surface modifications [45].

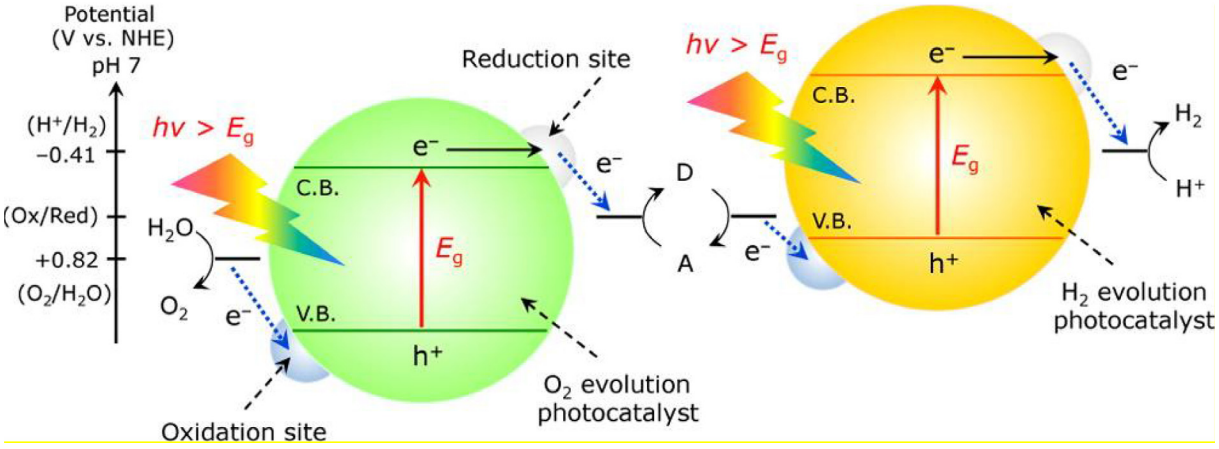

FIGURE 8

Schematic energy diagram of photocatalytic water splitting by a two-step photoexcitation system. C.B., conduction band; V.B., valence band; E_g, bandgap. D and A indicate electron donating and accepting species, respectively, Reproduced from ([176]) with permission. Copyright 2010, American Chemical Society.

TABLE 7

Z-scheme systems for water splitting under visible light irradiation.

H_2 photocatalyst	O_2 photocatalyst	Mediator	Activity/μmol h^{-1}		QY (%)	Refs. (Year)
			H_2	O_2		
$Ru/SrTiO_3/Rh$	$BiVO_4$	–	47.2	22.4	1.6 (420 nm)	[167] (2015)
$Pt/ZrO_2/TaON$	$RuO_2/TaON$	I^-/IO_3^-	10	4	–	[82] (2011)
$Rh/SrTiO_2$:(La/Rh)	$Ir/CoO_x/Ta_3N_5$	–	50	25	1.1 (420 nm)	[168] (2014)
$Pt–WO_3$	$Pt–BaTaO_2N$	I^-/IO_3^-	6	3	–	[169] (2009)
$Ru/SrTiO_3$:Rh	$BiVO_4$	$[Co(bpy)_3]^{3+/2+}$	100	47	2.1 (420 nm)	[170] (2013)
Coumarin-dye-adsorbed $Pt/H_4Nb_6O_{17}$	$IrO_2–Pt/WO_3$	I^-/I_3^-	2.42	1.2	<0.1 (500 nm)	[171] (2009)
$Pt/BaZrO_3–BaTaO_2N$	PtO_x/WO_3	I^-/IO_3^-	67.4	27.9	–	[47] (2013)
$Pt/ZrO_2/TaON$	$Ir/R–TiO_2/Ta_3N_5$	I^-/I_3^-	–	–	–	[172] (2010)
$Pt/SrTiO_3$:Rh	$BiVO_4$	Fe^{3+}/Fe^{2+}	122	61	4 (420 nm)	[46] (2013)
$Pt/SrTiO_3$:Cr/Ta	$PtO_x/H–Cs–WO_3$	I^-/I_3^-	32	16	1.5 (420 nm)	[46] (2013)
$Ru/Rh–SrTiO_3$	$Ru/Na,V–SrTiO_3$	I^-/IO_3^-	0.012	0.006	–	[173] (2012)
$Ru/SrTiO_3$:Rh	$IrO_x/SrTiO_3$:Rh/Sb	Fe^{3+}/Fe^{2+}	3	1.5	–	[48] (2014)
$Ru/SrTiO_3$:La,Rh	$RuO_x/BiVO_4$:Mo	Au	100	50	33 (419 nm)	[174] (2016)
$Ru/SrTiO_3$:La,Rh	$BiVO_4$:Mo	C	8	4	26 (419 nm)	[175] (2017)

Overall, in order to satisfy the band levels suitable for water reduction and oxidation, the single photocatalysts are mainly the oxide solid solutions or oxides and (oxy)nitrides solid solutions. At the same time, it is very essential to decorate them by the cocatalysts to provoke the separation of photogenerated electron-hole and increase the active sites pairs for the overall water splitting.

Z-scheme systems for water splitting

Z-scheme systems for water splitting use two different semiconductor photocatalysts, one for H_2 and the other for O_2 evolution separately, for example in Fig. 8. Typically, a shuttle redox mediator is necessary for the Z-scheme system. On the surface of H_2 evolution photocatalyst, the reduction sites transfer the conduction band electrons to hydrogen ions (H^+) to create H_2 and the electron donors (D) accept valence band holes to yield the corresponding electron acceptors (A) on the oxidation sites. On the other hand, the forward reactions on the O_2 evolution photocatalysts are for water oxidation by accepting the valence band holes on the oxidation sites and the electron acceptors (A) are regenerated to their reduced form (D) on the reduction sites. Consequently, a cycle of redox pairs (D and A) is necessary and the overall water-splitting reaction is achieved.

As shown in Table 7, the most frequent shuttles applied in the Z-scheme water splitting system are IO_3^-/I^-, I_3^-/I^- and Fe^{3+}/Fe^{2+}. (Oxy)nitrides and strontium titanate were regularly utilized as

the photocatalysts of H_2 evolution, while WO_3 and $BiVO_4$ as the other photocatalysts of O_2 evolution. Fig. 4 shows a typical Z-scheme water splitting system, in which RuO_2-decorated TaON as an O_2 evolution photocatalyst was combined with Pt-loaded ZrO_2/TaON as a H_2 evolution photocatalyst in an aqueous solution mixed with $NaIO_3$ and NaI [82].

There are many (oxy)nitrides applied in the Z-scheme system considering that the CB level of N 2p is higher than that of O 2p, resulting in the narrow bandgap and enhancing the photocatalytic activity. Tantalum nitride (Ta_3N_5), which was modified with nanoparticulate iridium (Ir) and rutile titania (R—TiO_2) as an O_2 evolution photocatalyst, was mixed with Pt–ZrO_2/TaON as a H_2 evolution photocatalyst to create a water splitting system in an IO_3^-/I^- shuttle redox mediator under visible light (λ >420 nm) [172]. Three mixed tantalum oxynitrides, $ATaO_2N$ (A = Ca, Sr, Ba), were applied in a Z-scheme water-splitting system as a H_2 evolution photocatalyst in combination with Pt–WO_3 as an O_2 evolution photocatalyst under visible light in the presence of IO_3^-/I^- shuttle redox [169]. $BaZrO_3$–$BaTaO_2N$ solid solution was also decorated with Pt nanoparticles as a hydrogen photocatalyst, and mixed with either PtO_x/WO_3 or TiO_2 rutile as water oxidation promoters in the presence of IO_3^-/I^- redox mediator, realizing Z-scheme water splitting under visible light irradiation [47].

Strontium titanate ($SrTiO_3$) is stable and photocorrosion-resistant, and its band gap and band structure are similar to those of TiO_2, so it has been widely applied as both the water reduction and oxidation catalyst in the photocatalytic water splitting under visible light. $SrTiO_3$ was used as the parental structure and doped with either vanadium (and sodium) as water reduction photocatalyst or rhodium as water oxidation photocatalyst to introduce visible light sensitivity in the presence of IO_3^-/I^- [173]. $SrTiO_3$ doped with rhodium was active only for H_2 evolution, but $SrTiO_3$ doped with rhodium and antimony with proper ratio was active for O_2 evolution as well, so a Z-scheme system composed of Ru/$SrTiO_3$:Rh and IrO_x/$SrTiO_3$:Rh/Sb was realized in the presence of Fe^{3+}/Fe^{2+} redox couple solution under visible light irradiation [48]. Using a hydrothermal method, a polymerizable complex method, and a solid-state reaction method to synthesis of $SrTiO_3$:Rh with different amounts of added Sr, another highly active Z-scheme system composed of $SrTiO_3$:Rh and $BiVO_4$ in the aqueous Fe^{3+}/Fe^{2+} solution was created as well [46]. Later, the Z-scheme system consisting of Ru/$SrTiO_3$:Rh and $BiVO_4$ was reported in the presence of $[Co(bpy)_3]^{3+/2+}$ and $[Co(phen)_3]^{3+/2+}$ electron mediators using a reaction cell in which the H_2 and O_2 evolution photocatalysts were divided with each other by a membrane filter [170]. A coumarin-dye-adsorbed lamellar niobium oxide as a hydrogen evolution photocatalyst and WO_3 as an O_2 evolution photocatalyst achieved sustainable water splitting under visible light with I_3^-/I^- used as a shuttle redox [171].

There were also some Z-scheme systems without addition of any electron mediator in the reaction solution. For instance, core/shell structured La- and Rh-codoped $SrTiO_3$ was combined with Ir/CoO_x/Ta_3N_5 for solar-light-driven Z-scheme water splitting [168]. At the same time, $BiVO_4$–$SrTiO_3$:Rh composites were also discovered for Z-scheme water splitting under simulated sunlight irradiation without electron mediators, in which $BiVO_4$ particles as an O_2 evolving photocatalyst was attached to Rh–$SrTiO_3$ particles as an H_2 evolving photocatalyst [167]. This simple composite photocatalyst got 1.6% quantum yield at 420 nm without additives, due to the formation of well-crystallized $BiVO_4$ single-crystal-like particles. Very recently, a Z-scheme system, based on La- and Rh-codoped $SrTiO_3$ and Mo-doped $BiVO_4$ powders embedded into a gold layer, enhanced the electron relay by annealing and suppressed undesirable reactions through surface modification, which allowed pure water splitting with a solar-to-hydrogen energy conversion efficiency (STH) of 1.1% and an apparent quantum yield (AQY) of over 30% at 419 nm at 331 K and 10 kPa [174]. Another similar system, a $SrTiO_3$:La, RhC/$BiVO_4$:Mo sheet was synthesized to achieve unassisted pure-water splitting with a STH of 1% and an AQY of 26% at a wavelength of 419 nm [175], which is so far the highest among Z-scheme pure water splitting operating at ambient pressure.

From above one can see, an efficient Z-scheme system for water splitting under solar light irradiation requires suitable shuttles for electron and hole exchange, between reduction and oxidation photocatalysts. Furthermore, the proper levels of conduction and VBs and desirable crystal structures can ensure and improve the performance of a Z-scheme system in visible light-driven water splitting.

Advancements in carbon-based organic semiconductor photocatalyst for water redox

Apart from metal-based photocatalysts (such as inorganic semiconductors or organometal complexes), the discovery of carbon based organic semiconductor photocatalysts for visible light-driven water splitting has recently triggered a great interest [3,155]. Compared to inorganic materials, the family of organic materials possesses great advantages, such as light-weight, a wealth of element resource supplement, diversity of fabrication approaches, structural control and flexibility, chemically tunable electronic and optical properties, and low cost [3,155]. Till now, enormous organic and carbonaceous materials have been developed for photocatalytic water splitting, including carbon nitride, graphene oxide (GO), heteroatom-doped graphene, boron carbide, hexagonal boron carbon nitride (h-BCN), conjugated polymers, as well as non-covalent self-assembly supramolecular systems. Careful manipulation and detailed investigation in the optical band gap, HOMO–LUMO energy levels, thermodynamic driving force, charge carrier mobility, surface area, and interface wettability are vital to pursue efficient new photocatalysts for visible light-driven water splitting [177].

This section provides a summary of the progress of carbon-based organic semiconductor photocatalyst for water redox reactions, with special highlights on the primary synthetic approaches, molecular design principles, and the relationship of structure and performance.

Melon-based carbon nitride photocatalysts

The keen interest of carbon nitride polymer as a photocatalyst for water splitting reaction has been aroused recently since its first report as a polymer photocatalyst for water splitting reaction in 2009 [178–180]. This carbon nitride is a π-conjugated polymeric semiconductor material that possesses a graphite-like sp^2-bonded C—N structure with tri-*s*-triazine (melem) as the basic building

TABLE 8

Carbon nitride photocatalysts for hydrogen evolution under visible light illumination.

Photocatalyst	Cocatalyst	Reactant solutions	Light source	Hydrogen evolution rate/μmol h^{-1}	QY (%)	Ref. (Year)
$P_3HT/g\text{-}C_3N_4$	Pt	Ascorbic acid	Xe-300 W, >420 nm	3045	77.4 (420 nm)	[166] (2015)
$g\text{-}C_3N_4\text{–}Pt^{2+}$	–	TEOA	Xe-300 W, >400 nm	60.49	–	[53] (2016)
$g\text{-}C_3N_4$ nanosheets	Pt	TEOA, K_2HPO_4	Xe-300 W, L40 cutoff filter	947	26.1 (420 nm)	[185] (2015)
$g\text{-}C_3N_4$/nitrogen-rich carbon nanofibers	–	TEOA	Xe-300 W, >420 nm	169	14.3 (420 nm)	[181] (2016)
Nanospherical $g\text{-}C_3N_4$ composed of nanosheets	Pt	TEOA	Xe-300 W, >420 nm	574	9.6 (420 nm)	[186] (2014)
ATCN modified $g\text{-}C_3N_4$ nanosheets	Pt	TEOA	Xe-300 W, >420 nm	85	8.8 (420 nm)	[186] (2014)
CdS–Au–HCNS	Pt	TEOA	Xe-300 W, >455 nm	277	8.7 (420 nm)	[187] (2015)
$g\text{-}C_3N_4$ "seaweed"	Pt	TEOA	Xe-300 W, >420 nm	99	7.8 (420 nm)	[53] (2015)
Hollow spherical $g\text{-}C_3N_4$ (HCNS-1)	Pt	TEOA	Xe-300 W, >420 nm	224	7.5 (420 nm)	[112] (2012)
Phosphoric acid protonated porous $g\text{-}C_3N_4$ nanosheets	Pt	TEOA	Xe-300 W, >400 nm	195.8	6.1 (420 nm)	[80] (2016)
Porous P-doped $g\text{-}C_3N_4$ nanosheets	Pt	TEOA	Xe-300 W, >400 nm	80	3.56 (420 nm)	[188] (2015)
3 wt% poly(3-hexylthiophene)–$g\text{-}C_3N_4$	Pt	$Na_2S\text{–}Na_2SO_3$	Mercury lamp-300 W, >400 nm	560	2.9 (420 nm)	[189] (2011)
Self-sensitized carbon nitride microspheres(SSCN)	Pt	TEOA	Xe-300 W, >420 nm	4.96	1.07 (420 nm)	[190] (2016)
Defect-modified $g\text{-}C_3N_4$ (DCN-200)	Pt	TEOA	Xe-300 W, >420 nm	100	–	[65] (2016)
$g\text{-}C_3N_4$ photonic crystals	Pt	TEOA	Xe-300 W, >420 nm	40	–	[191] (2016)
Layered $g\text{-}C_3N_4$ obtained at 580 °C	Pt	TEOA	Xe-300 W, >440 nm	29.9	–	[192] (2016)
Bulk $g\text{-}C_3N_4$	Pt	TEOA	Xe-300 W, >420 nm	10.7	0.1 (420–460 nm)	[178] (2009)
Urea-derived $g\text{-}C_3N_4$	Pt	TEOA	Xe-300 W, >395 nm	66.55	26.5 (400 nm)	[193] (2014)

unit connected by planar amino groups [177]. This polymer can be synthesized by thermal polymerization of nitrogen-rich precursors (*e.g.*, cyanamide, dicyandiamide, melamine, urea, or mixtures). Based on the electronic structure calculated by density functional theory, the carbon and nitrogen atoms serve as the preferred sites for proton reduction to H_2 and water oxidation to O_2, respectively [178]. The band positions of carbon nitride are located energetically favorable for water splitting, because the bandgap of carbon nitride polymer was measured to be 2.7 eV with the CB at −1.31 V and VB at 1.49 V *vs.* NHE [178].

Although carbon nitride polymer has been recognized as a promising photocatalyst for water reduction, the hydrogen evolution rate of bulk carbon nitride polymer is generally low in comparison with other inorganic photocatalysts even with the use of noble metal co-catalysts. The major problems originate from: (1) limited visible light absorption due to the relatively large bandgap of melon-based carbon nitride; (2) fast recombination of photogenerated electron-hole pairs owing to the high exciton binding energy and the low charge mobility; and (3) low proton reduction efficiency on its surface as a result of the covalent bonding nature in carbon nitride. To overcome these bottlenecks, a variety of techniques have been developed to increase the hydrogen evolution rate, including heteroatom doping, copolymerization, defect modification, loading cocatalysts, pore structure creation, nanostructure engineering, homojunction and heterojunction design, as well as dye sensitization.

Table 8 lists the representative summary of carbon nitride photocatalysts for hydrogen evolution under visible light irradiation. Impressively, the development of metal-free composite photocatalysts provides effective pathways for optimizing the hydrogen evolution activity of polymeric carbon nitride semiconductor. Qu and coworkers demonstrated an interconnected framework of mesoporous carbon nitride nanofibers merged with nitrogen-rich carbon for efficient photocatalytic hydrogen evolution without cocatalysts [181]. The composition and structure of the nanofibers as well as strong coupling between the components was reported by the authors to lead to better light-harvesting properties, improved charge separation, and a multidimensional electron transport path that improve the hydrogen evolution activity [181]. The as-synthesized catalyst exhibits a QY of 14.3 % at 420 nm without any cocatalysts [181]. Additionally, the creation of homojunction structures by the defect-induced self-functionalization also constitutes a promising strategy to realize precise band engineering of carbon nitride for more

efficient water splitting. Defect-modified carbon nitride (DCN) photocatalysts, which was synthesized via a low-temperature heating (<350 °C) of carbon nitride with $NaBH_4$ under an inert atmosphere, showed much extended light absorption with band gaps decreased from 2.75 to 2.00 eV [182]. The introduction of cyano terminal C≡N groups (acting as electron acceptors) into the DCN sheet edge rendered the DCN with both n- and p-type conductivities, and consequently induced the generation of p–n homojunction [182]. This homojunction structure accelerated charge transfer and separation, resulting in a fivefold improved photocatalytic H_2 evolution ability [182].

Polymeric carbon nitride photocatalysts have also shown a great potential in water oxidation half-reaction. However, the photocatalytic O_2 evolution reaction on carbon nitride is low because of the poor charge separation efficiency and sluggish surface kinetics due to the relatively negative LUMO position of the carbon nitride semiconductor determined by the N 2p hybridization. Thus, there is a great necessity to improve the water oxidation activity of the polymer photocatalysts by electronic structure modulation, heterostructure construction and cocatalyst design. For instance, carbon nitride matrix was deposited with layered $Co(OH)_2$ for photocatalytic water oxidation with UV–vis and visible light illumination [166]. The optimum oxygen evolution rate of the $Co(OH)_2$-modified carbon nitride sample reached 27.4 and 7.1 μmol h^{-1} under UV–vis (λ >300 nm) and visible light (λ >420 nm) irradiation, which are 5.5 and 7 times higher than those for pristine one, respectively [166]. This cocatalyst modification protocol not only promotes the interface transfer rate of charge carriers, but also lowers the excessive energy barrier for O—O formation, thus leading to enhanced reaction kinetics for photocatalytic water oxidation [166], carbon nitride matrix was deposited with layered $Co(OH)_2$ for photocatalytic water oxidation with UV–vis and visible light illumination. The optimum oxygen evolution rate of the $Co(OH)_2$-modifed carbon nitride sample reached 27.4 and 7.1 μmol h^{-1} under UV–vis (λ >300 nm) and visible light (λ >420 nm) irradiation,

TABLE 9

g-C_3N_4 based photocatalysts for overall water splitting under visible light irradiation.

Photocatalyst	Light source	H_2 evolution rate/ μmol h^{-1}	O_2 evolution rate/ μmol h^{-1}	QY (%)	Refs. (Year)
Pt–g-C_3N_4, Fe^{3+}/Fe^{2+}, $BiVO_4$	Xe-300 W, >395 nm	6	3	–	[52] (2014)
Pt–g-C_3N_4, IO_3^-/I^-, Pt–WO_3	Xe-300 W, >395 nm	21.2	11.0	–	[52] (2014)
Pt–g-C_3N_4–rGO–WO_3	Iron doped metal halide lamp-250 W, >420 nm	2.84	1.46	0.9 (420 nm)	[194] (2015)
TiO_2/C_3N_4(Pt),IO_3^-/I^-, β-$Ni(OH)_2/WO_3(PtO_x)$	Xe-150 W, full arc	50.2	24.3	4.94 (365 nm) 4.01 (405 nm) 2.06 (425 nm)	[195] (2016)
Carbon nanodots/g-C_3N_4 nanosheets	Xe-300 W, >420 nm	8.4	4.1	16 (420 ± 20 nm) 6.2(580 ± 15 nm) 4.42(600 ± 10 nm)	[185] (2015)
Pt/g-C_3N_4 nanowire bundles (CN NWB)	Xe, >420 nm	3.6	1.78	5.2 (420 nm)	[183] (2016)
Pt–PtO_x–CoO_x/g-C_3N_4 nanosheets	Xe-300 W, >300 nm Xe-300 W, >420 nm	12.2 1.2	6.3 0.6	0.3 (405 nm)	[181] (2016)

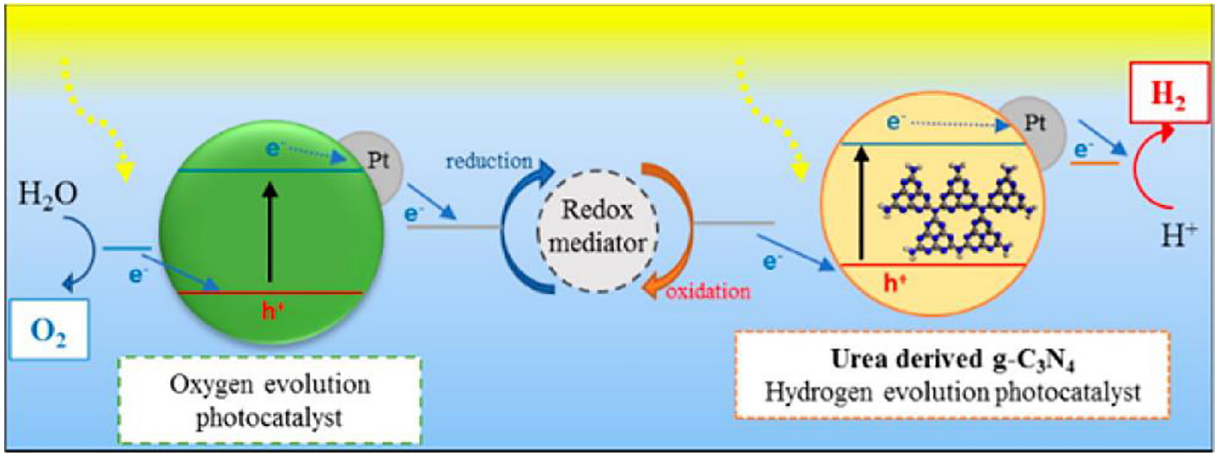

FIGURE 9

Schematic diagram of photogenerated electron transfer in a nature-inspired water splitting system. Urea derived g-C_3N_4 worked as the hydrogen evolution and two different metal oxides, $BiVO_4$ and WO_3, served as the O_2 evolution photocatalyst under UV/visible light irradiation [52]. Copyright 2014, American Chemical Society.

which are 5.5 and 7 times higher than those for pristine one, respectively. This cocatalyst modification protocol not only promotes the interface transfer rate of charge carriers, but also lowers the excessive energy barrier for O—O formation, thus leading to enhanced reaction kinetics for photocatalytic water oxidation.

Apart from the utilization of carbon nitride photocatalyst in water splitting half-reactions, it is a vital challenge to establish photocatalytic overall water splitting system by using carbon nitride polymers in the absence of sacrificial reagent. Table 9 lists the reported g-carbon nitride photocatalysts for overall water splitting under visible light irradiation. One of the feasible pathways to realize direct pure water splitting is by rational synthesis of carbon nitride matrix and modification with appropriate cocatalysts [183]. For example, Pt and Co_3O_4 nanoparticles were specifically loaded onto the interior and exterior surface of hollow carbon nitride spheres (HCNS), respectively, to optimize the surface redox functions of the polymer semiconductors for overall water splitting [184]. A steady evolution of H_2 and O_2 in a nearly stoichiometric ratio ($H_2/O_2 = 2.1$) was realized on the HCNS photocatalyst with the Pt and Co_3O_4 cocatalysts loaded on the inner and outer surfaces. Additionally, the rate of gas evolution increased to ~10 times faster than pure HCNS (0.3 μmol h^{-1} H_2 and 0.2 μmol h^{-1} O_2) and to 3 times faster than that of the random distribution of Pt and Co_3O_4 cocatalysts on the HCNS outer surface with the same loading amount. The improved activity was due to the spatially separated reactive sites for the evolution of H_2 and O_2 and the unidirectional transfer of the electron and hole on the surfaces, thus inhibiting the unwanted reverse reaction and reducing charge recombination. Another strategy is to develop a Z-scheme overall water splitting system, which is composed of two semiconductor photocatalysts and the closely related redox processes. An overall water splitting system under visible light irradiation has been constructed involving Pt–g-C_3N_4/WO_3 and soluble redox mediator (IO_3^-/I^- pairs) (Fig. 9) [52]. A stable and reproducible hydrogen evolution rate and oxygen evolution rate at 36 and 18 μmol h^{-1} g^{-1} (in a ratio of 2:1) from water was tested over 14 h under full arc, and average rates of 21.2 and 11.0 μmol h^{-1} g^{-1} of H_2 and O_2 are observed under visible irradiation (λ >395 nm) [52]. A higher efficiency for pure water splitting was reported for the carbon–nanodots/carbon–nitride nanocomposite, but it seems further works are needed to confirm reproducibility [185].

To sum up, a large amount of carbon nitride based materials with enhanced activity have been developed for photocatalytic water splitting. These works will pave new pathways for the construction of organic photosynthetic units for the sustainable utilization of solar energy [72].

Crystalline carbon nitride photocatalysts

Highly crystalline and fully condensed carbon nitride materials hold a great prospect for photocatalytic water splitting due to the optimized structure and the minimized defects (acting as recombination centers for electron-hole pairs) than the common melon-based carbon nitride polymers. For such a highly crystalline carbon nitride material, it could be generally named as graphitic carbon nitride (g-C_3N_4) to distinguish from melon-based carbon nitride polymers. So far, there have been a handful of crystalline carbon nitride photocatalysts for water splitting, such as poly(triazine imide) (PTI), tri-*s*-triazine-based g-C_3N_4 and poly(heptazine imide). Table 10 lists the crystalline carbon nitride photocatalysts reported for hydrogen evolution under visible light illumination. These highly crystalline and sufficiently condensed carbon nitride materials are usually synthesized via salt melt method, because the molten salt can not only act as a solvent for high-temperature materials synthesis involving complex organic and inorganic reactions, but also as a structure directing agent to manipulate texture and porosity of the products.

PTI is one of the crystalline g-C_3N_4 materials that shows photocatalytic activity for water splitting. A carbon nitride intercalation compound was obtained by heating melamine with a low melting point eutectic mixed salts (LiCl·H_2O–KCl–NaCl) under air and ambient pressure [196]. The as-obtained g-C_3N_4 nanotubes exhibited a high QY of 21.2% at 420 nm for photocatalytic H_2 evolution in TEOA aqueous solution [196]. The improvement in hydrogen generation was attributed to the

TABLE 10

Crystalline carbon nitride photocatalysts for hydrogen evolution half-reaction under visible light illumination.

Photocatalyst	Co-catalyst	Reactant solutions	Light source	H_2 evolution rate/μmol h^{-1}	QY (%)	Ref. (Year)
CN(Li–K)	Pt	TEOA	Xe-300 W, >300 nm Xe-300 W, >420 nm	80 0.14	–	[202] (2013)
Carbon nitride intercalation compound (CNIC) nanotubes	Pt	TEOA	Xe-300 W, >420 nm	346	21.2 (420 nm)	[196] (2013)
Crystalline carbon nitrides, PTI-0.13	Pt	TEOA	Xe-300 W, >420 nm	204	15 (400 nm) 7 (420 nm)	[203] (2014)
Triazine-based PTI nanosheets	Pt	TEOA	Xe-300 W, >420 nm	3.5	1.3 (400 nm)	[204] (2014)
PTI-0.15	Pt	TEOA	Xe-300 W, 385–740 nm	13	–	[197] (2015)
Dendritic tip-on carbon nitride PTI-0.15/KCC-1	Pt	TEOA	Xe-300 W, 385–740 nm	33	22.1 (400 nm) 16.9 (420 nm)	[197] (2015)
Tri-*s*-triazine-based g-C_3N_4	Pt	TEOA	Xe-300 W, >420 nm	73.6	–	[198] (2016)
Tri-*s*-triazine-based g-C_3N_4	Pt	TEOA,K_2HPO_4	Xe-300 W, >420 nm	770	50.7 (405 nm)	[198] (2016)
3-Amino-1,2,4-triazole-5-thiol (II-LiK-CN)	Pt	TEOA	LED-50 W, >420 nm	20.3	–	[200] (2015)
Guanazole (I-LiK-CN)	Pt	TEOA	LED-50 W, >420 nm	3.3	–	[200] (2015)
MoS_2/poly(heptazine imide)	–	TEOA	LED-50 W, >420 nm	1.34	–	[201] (2016)
MoS_2/Co_2O_3/poly(heptazine imide)	–	TEOA	LED-50 W, >420 nm	0.67	–	[201] (2016)

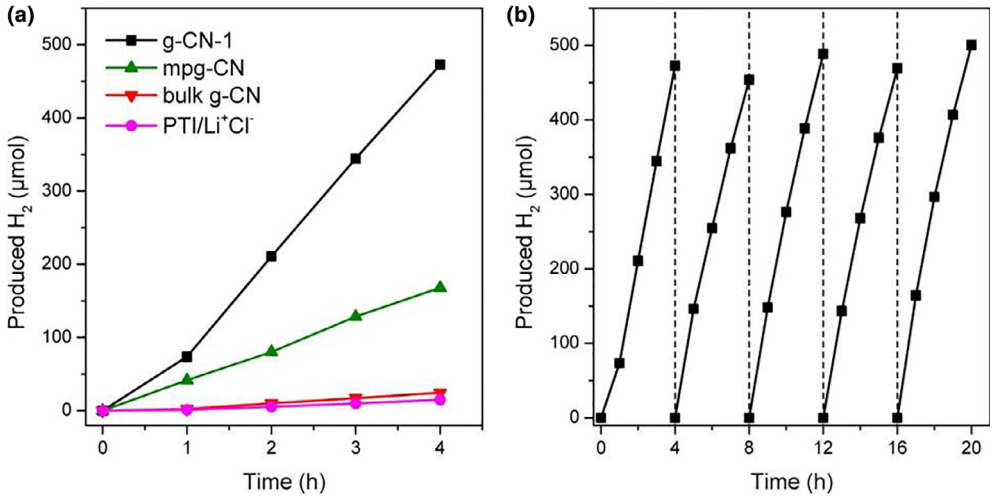

FIGURE 10

Hydrogen production of the samples and stability test for g-CN-1 under visible light (λ >420 nm) irradiation using TEOA (a and b) as the sacrificial agents. Reprinted with permission from Ref. [198], Copyright 2016, American Chemical Society.

greatly accelerated transportation and separation of photogenerated carriers after inserting the alkali metal salts into the interlayer of g-C_3N_4 [196]. Bhunia et al. prepared triazine-based carbon nitride materials with different C/N ratios by a two-step synthesis procedure: starting with the solution state dispersion of the monomers via hydrogen-bonding supramolecular aggregate of melamine and 2,4,6-triaminopyrimidine, followed by a salt-melt thermal polycondensation [197]. Moreover, the photocatalytic activity was further promoted by providing a dendritic tip-on-like shape grown on porous fibrous silica KCC-1 spheres, and photo-depositing with highly dispersed Pt nanoparticles (<5 nm) [197]. Consequently, the photocatalyst of Pt/PTI/KCC-1 exhibited a QY of 22.1 ± 3% at 400 nm for hydrogen evolution [197]. This finding provides a feasible pathway for the production of viable crystalline carbon nitride by combining salt melt method with supramolecular pre-organization of precursor, copolymerization, and nanostructure design.

Tri-*s*-triazine-based g-C_3N_4 is also a promising photocatalyst owing to its extended and fully condensed conjugated structure, which stabilizes the π-electron system for a fast charge mobility and improves the sunlight-harvesting capability [198]. A crystalline tri-*s*-triazine-based g-C_3N_4 (g-CN-1) was prepared using preheated melamine as a precursor and the salt melt method (Fig. 10) [198]. The SEM images of g-CN-1 sample exhibited a nanosheet to nanorod structure with a porous structure, and the high-resolution TEM images reveals a clear hexagonal lattice structure of the crystal with two lattice fringes [198]. The lattice fringe corresponding to 0.33 nm might be assigned as the interlayer distance, and the other corresponding to 0.98 nm was likely originated from the in-plane periodicity [198]. The g-CN-1 sample exhibited a high stability and photocatalytic activity toward hydrogen and oxygen production from water splitting [198]. Impressively, a high QY of 50.7% at 405 nm for hydrogen production has been achieved on tri-*s*-triazine-based g-C_3N_4 by adding phosphate to mimic natural photosynthetic environment [198].

Poly(heptazine imide), which reveals a two-dimensional planar heptazine-based network containing isolated melamine molecules in the trigonal voids, has been recently used as a photocatalyst for water splitting [199]. Partially negatively charged potassium poly(heptazine imides) was prepared by the pyrolysis of 3,5-disubstituted-1,2,4-triazole derivatives, 3,5-diamino-1,2,4-triazole and 3-amino-1,2,4-triazole-5-thiol in LiCl/KCl salt melts [200]. The potassium poly(heptazine imides) exhibited a high photocatalytic activity in hydrogen evolution reaction upon visible light irradiation with a Pt cocatalyst[200]. Furthermore, MoS_2/Co_2O_3/poly(heptazine imide) composites were also prepared by ionothermal condensation of 3-amino-1,2,4-triazole-5-thiol, using small quantities of $MoCl_5$ and a reactive Co precursor for the introduction of MoS_2 nanoparticles and cobalt species, respectively [201]. The materials were active in both noble-metal-free water reduction and water oxidation half reactions upon visible light irradiation [201]. MoS_2/Co_2O_3/poly(heptazine imide) exhibited 10% of the hydrogen evolution activity of a reference Pt/g-C_3N_4 composite, and half of the oxygen evolution rate of the reference Co_3O_4/S-doped carbon nitride material [201].

In summary, a series of crystalline carbon nitride photocatalysts for half reactions in water splitting, including poly(triazine imide) (PTI), tri-*s*-triazine-based g-C_3N_4 and poly(heptazine imide) have been prepared from the salt molten synthetic process. By tailoring the crystallinity and conjugated subunits of the carbon nitride photocatalysis, crystalline carbon nitride compounds are anticipated to show a great potential to solar energy applications, such as water splitting, CO_2 photofixation, organic photosynthesis, and pollutant degradation.

Graphene oxide (GO) and heteroatom doped graphene based photocatalysts

Graphene, a single-atom-thick planar sheet of sp^2 hybridized carbons that are densely bound in a hexagonal lattice, has received a considerable interest owing to its unique physical and chemical properties [205]. However, the (half)-metallic feature and zero bandgap nature of pristine graphene limits its direct application as a photocatalyst [205]. In most of the studies, graphene is used

as an electron acceptor or conductor to combine with other semiconductors forming composite photocatalysts for water splitting [205].

Graphene oxide (GO) has a wider bandgap than graphene, and may serve as a potential candidate for photocatalytic water splitting [206]. GO semiconductor with an apparent bandgap of 2.4–4.3 eV was synthesized by a modified Hummers' procedure [206]. Under UV or visible light irradiation, GO photocatalyst steadily catalyzes H_2 production from a 20 vol.% methanol aqueous solution and pure water [206]. Nevertheless, the p-type conductivity of GO hinders photogenerated hole transfer for water oxidation and prohibits O_2 evolution. To overcome this problem, a n-type N-containing GO semiconductor was synthesized by treating GO with NH_3 gas at room temperature to introduce amino and amide groups into its surface [207]. The N-containing GO effectively accelerates the transfer of photogenerated holes for photocatalytic oxygen evolution and suppressed H_2 evolution in a methanol aqueous solution [207]. N-containing GO exhibited the ability to simultaneously catalyze H_2 and O_2 evolutions from pure water under visible light irradiation, but with a H_2/O_2 molar ratio below 2 [207]. Rationally controlling the degree of oxidation, size, morphology, and composition is expected to modify the electronic structure, optical properties, and photocatalytic performance of GO [205].

Heteroatom (*e.g.*, B, N, P, F, Cl, Br, I)-doped graphene is a kind of graphene-based photocatalyst for water splitting, because heteroatom doping in ideal graphene sheets could open up their bandgap and transform zero bandgap graphene into a semiconductor. For example, P-doped graphene (denoted as (P)G) photocatalyst was synthesized by pyrolysis of $H_2PO_4^-$ modified alginate (an abundant and natural oligosaccharide) at 900 °C under an inert [208]. The optical bandgap and the photocatalytic performance of (P)G increase with the P content [208]. The hydrogen evolution rate increased greatly with the percentage of $H_2PO_4^-$ introduced during the preparation of (P)G, and the (P)G-4 sample prepared with the maximum percentage of $H_2PO_4^-$ showed the best photocatalytic activity of 12 μmol $g^{-1}h^{-1}$ H_2 evolution rate [208]. The optimal (P)G-4 photocatalyst exhibited a much higher hydrogen evolution rate than both GO and graphene of below 2 μmol g^{-1} h^{-1} H_2 evolution rate under UV/Vis illumination from water/methanol mixtures [208]. TEOA as the hole scavenger also largely promoted the H_2 evolution rate to 300 μmol g^{-1} h^{-1} under the same experimental conditions for (P)G-4 [208]. More highly efficient photocatalysts based on heteroatom doped graphene are envisaged via manipulation of the type of

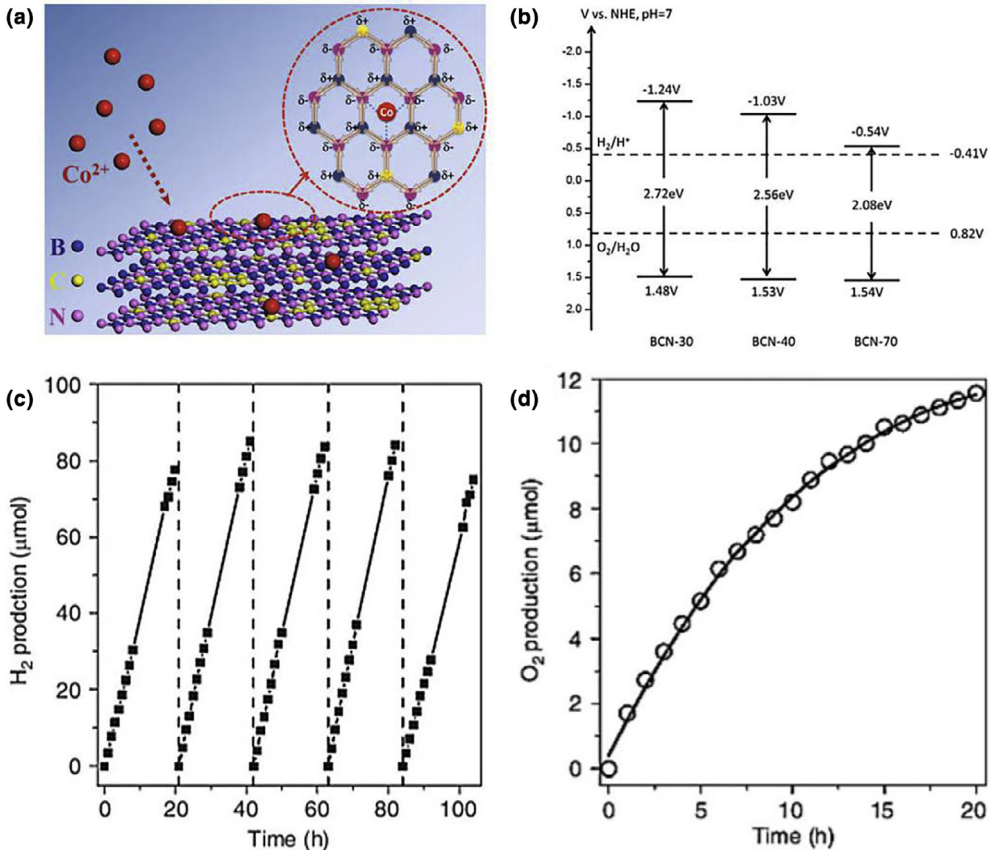

FIGURE 11

(a) Chemical structure of Co^{2+}/*h*-BCN. (b) The determined band structure of BCN-x, where x (30, 40, 70) is the percentage weight content of glucose to boron oxide, with respect to normal hydrogen electrode (NHE). (c) Stable hydrogen evolution from water by of *h*-BCN under visible light. The reaction continued for 104 h, with evacuation every 20 h (dashed line). (d) Time courses of oxygen production from water by Ni-Co LDHs/*h*-BCN under visible light illumination (λ >420 nm). Reprinted with permission from Ref. [166], Copyright 2015, Springer-Verlag. Reprinted with permission from Ref. [210], Copyright 2015, Nature Publishing Group.

dopants and their bonding configurations in the graphene framework [205]. Benefiting from the advantages of wide availability, sustainability, and easy derivatization, the use of graphene-like materials as photocatalysts provides new avenue for solar energy conversion.

Boron carbide and hexagonal boron carbon nitride (h-BCN) photocatalysts

Boron carbide and hexagonal boron carbon nitride (*h*-BCN) are interesting new class of efficient metal-free photocatalysts for water splitting reaction. Two boron carbides ($B_{4.3}C$ and $B_{13}C_2$) were developed as photocatalysts for H_2 production [209]. The hydrogen evolution rate over $B_{4.3}C$ reached ca. 14.5 μmol h^{-1} g^{-1}, which is over 3 times larger than that over $B_{13}C_2$ (4.5 μmol h^{-1} g^{-1}) without metal co-catalysts [209]. The structural defects and distortions in boron carbide were the main factors that affected their band structures and photocatalytic abilities for water splitting [209].

Besides that, *h*-BCN, formed by carbon doping of layered hexagonal boron nitride nanosheets, has also emerged as an active photocatalyst for water splitting under visible light irradiation (Fig. 11b and c) [210]. Based on theoretical and experimental investigations, the visible light absorption and emission with tunable wavelength could be realized via manipulating the carbon content in (B, N) rich *h*-BCN nanostructures. *h*-BCN materials with different amounts of incorporated carbon were synthesized by a pyrolysis method via heating the mixture of glucose, boron oxide and urea in an ammonia atmosphere at 1250 °C for 5 h [210]. Meanwhile, the bandgap of ternary *h*-BCN could be effectively narrowed by doping aromatic carbon into the boron nitride lattice (Fig. 11b) [210]. The most active BCN-30 exhibited an appropriate band structure (bandgap ≈ 2.72 eV, CB ≈ −1.24 V, VB ≈ 1.48 V *vs.* NHE at pH 7), straddling potentials of both water reduction and water oxidation [210]. In the hydrogen evolution studies, BCN-30 showed a hydrogen evolution rate of 6.0 μmol h^{-1} when loaded with 3 wt.% Pt cocatalyst, and 3.6 μmol h^{-1} without a cocatalyst under visible light (λ >420 nm) (Fig. 11c) [210]. The AQY of 1.0 wt% Pt-loaded BCN-30 was calculated to be 0.54% at 405 nm. In the water oxidation array, the Ni-Co-layered double hydroxides (Ni-Co LDHs)/*h*-BCN catalyst liberated 11 μmol O_2 in 20-h reaction with visible light, and generated 35 μmol O_2 with UV light [210]. Similarly, after intercalating cobalt ions in the *h*-BCN host, the synergic catalysis improved charge separation and lowered reaction barriers, hence promoting the photocatalytic water oxidation activity of the layered Co/*h*-BCN hybrid (Fig. 11a and d) [166]. The *h*-BCN with high specific surface area showed a strong chemical affinity toward metal ions owing to the "lop-sided" densities feature of ionic B—N bonding, enabling the generation of metal/h-BCN composite-layered structures with unique properties [166]. These sustainable photocatalysts composed of lightweight elements show great potential for the innovative creation of photoredox cascades for solar energy utilization and conversion [166].

Conjugated polymer photocatalysts

Conjugated polymers, such as π-conjugated linear polymers, heptazine-based microporous polymer networks, covalent triazine frameworks, covalent organic frameworks (COF), and conjugated porous polymers, represent a new generation of organic photocatalysts for water splitting [204,211,212].

Cooper et al. developed 15 polymer networks using Pd(0)-catalyzed Suzuki–Miyaura polycondensation of 1,4-benzene diboronic acid (1) and/or 1,3,6,8-tetraboronic pinacol ester of pyrene (3) and/or 1,2,4,5-tetrabromobenzene (2) and/or 1,3,6,8-tetrabromopyrene (4) [213]. The optical gap in a series of microporous copolymers was finely manipulated over a broad range (1.94–2.95 eV) by varying monomer composition [213]. The amorphous, microporous organic polymers with specific monomer compositions can act as robust and effective photocatalysts for H_2 evolution in the presence of a sacrificial electron donor, without the apparent need for an additional metal cocatalyst [213]. Wang and Zhang et al. developed a variety of conjugated polybenzothiadiazoles polymers with defined energy-band structures and charge-transfer and charge-separation abilities by copolymerizing the electron withdrawing benzothiadiazole units at different positions on phenyl rings (Fig. 12) [214]. Photocatalytic H_2 evolution efficiencies up to 116 μmol h^{-1} and an QY of 4.01 % at 420 nm were observed by employing the linear polymer based on a phenyl-benzothiadiazole alternating main chain with TEOA as the sacrificial agent [214]. The superior activity of its light-induced charge-transfer, charge-separation, and electron-transfer ability were the main reasons that contributed to the superior catalytic efficiency of the linear polybenzothiadiazole [214]. Additionally, a series of 2D azine-linked COFs were also prepared using a triphenylene platform that was modified for photocatalytic water reduction through a molecular design (Fig. 12) [215]. The building blocks were composed of hydrazine and triphenylarylaldehydes with different numbers (0–3) of nitrogen atoms in the central aryl ring [215]. Although all four COFs exhibited an optical bandgap between 2.6 and 2.7 eV and similar optical absorption profiles, a gradual enhancement in porosity and crystallinity from N_0—COF to N_3—COF was observed with the increase in nitrogen content and the planarity of the building blocks resulted [215]. A 4-fold increase in H_2 evolution was detected under visible light irradiation with each isolable substitution of C—H by N in the central aryl ring of the COF platform [215]. The average amount of H_2 produced by the series N_0, N_1, N_2, and N_3—COF was found to be 0.1, 0.4, 2.2, and 8.5 μmol h^{-1}, respectively [215]. The integration of the salient features, such as crystallinity, porosity, stability, and the ability of extended visible light harvesting, contribute to the genesis of COFs capable of photocatalytic hydrogen evolution [216]. Especially, 1,3-diyne-linked conjugated microporous polymer nanosheets (CMPNs) prepared by 1,3,5-tris(4-ethynylpheyl)-benzene (TEPB) and 1,3,5-triethynylbenzene (TEB) respectively, could act as highly efficient photocatalysts for pure water (pH ≈ 7) into stoichiometric amounts of H_2 and O_2 under visible light [217]. The apparent quantum efficiencies at 420 nm are 10.3% and 7.6% for CMPNs synthesized from TEPB and TEB, respectively; the measured solar-to-hydrogen conversion efficiency using the full solar spectrum could reach 0.6%, surpassing photosynthetic plants in converting solar energy to biomass (globally average ≈0.10%) [217].

Taking account of the wide number of organic compounds and the variety of structural variations which can be made

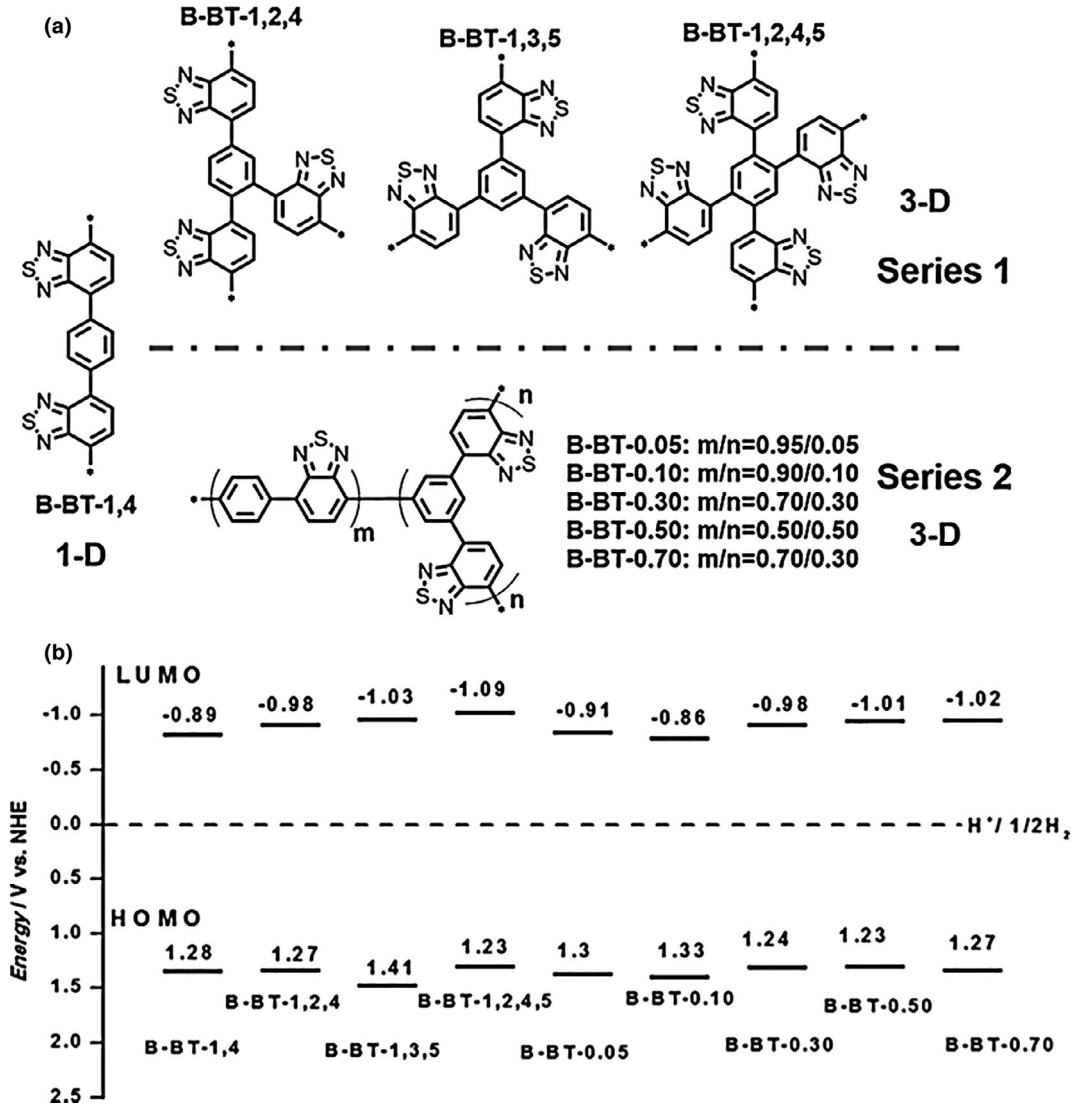

FIGURE 12

(a) Structures of two series of polybenzothiadiazoles with different molecular designs. (b) HOMO and LUMO band position of the polymers (the standard error of LUMO position is ±0.008 eV from three measurements). Reprinted with permission from Ref. [214], Copyright 2016, Wiley-VCH Verlag.

synthetically, the development of more efficient conjugated polymer photocatalysts for enhanced water splitting, by photosynthesis, is envisaged [183].

Supramolecular organic photocatalysts

Compared to the COFs, non-covalent self-assembly supramolecular system composed of purely perylene-3,4,9,10-tetracarboxylic diimide (PDINH) organic molecules was also used as a photocatalyst for visible light-driven water oxidation [182]. The photocatalyst has a bandgap of 2.20 eV, a CB at −0.049 V, and a VB at 2.20 V *vs.* NHE. Upon visible light irradiation, photo-induced electrons tend to migrate along the long-range transport pathway through charge delocalization, whereas holes spread out over self-assembled PDINH supramolecular system with nanoscale thickness to oxidize water into oxygen, resulting in an effective spatial charge separation. The amount of produced oxygen reached 1.29 μmol after 10 h of reaction in the presence of $AgNO_3$ electron acceptor with visible light (λ >420 nm) irradiation. The photocatalytic activity of the PDINH supramolecular system was attributed to the band-like electronic energy-level structure, which originated from orbital overlaps between PDINH molecular units and long-range conjugated π-delocalization within the self-assembled PDINH supramolecular system. Their findings will pave new pathways for photocatalysis based on self-assembled supramolecular systems.

Advancements in the semiconductor-coordination compound systems for water splitting

Coordination compounds have regarded to play multiple functions in the photocatalytic water splitting processes. They can serve either as (i) photocatalysts (light absorbers) alone or in combination with semiconductor particles; (ii) electron transfer mediators facilitating the charge transfer between the photosensitizer and catalytic centers or between two photoactive compo-

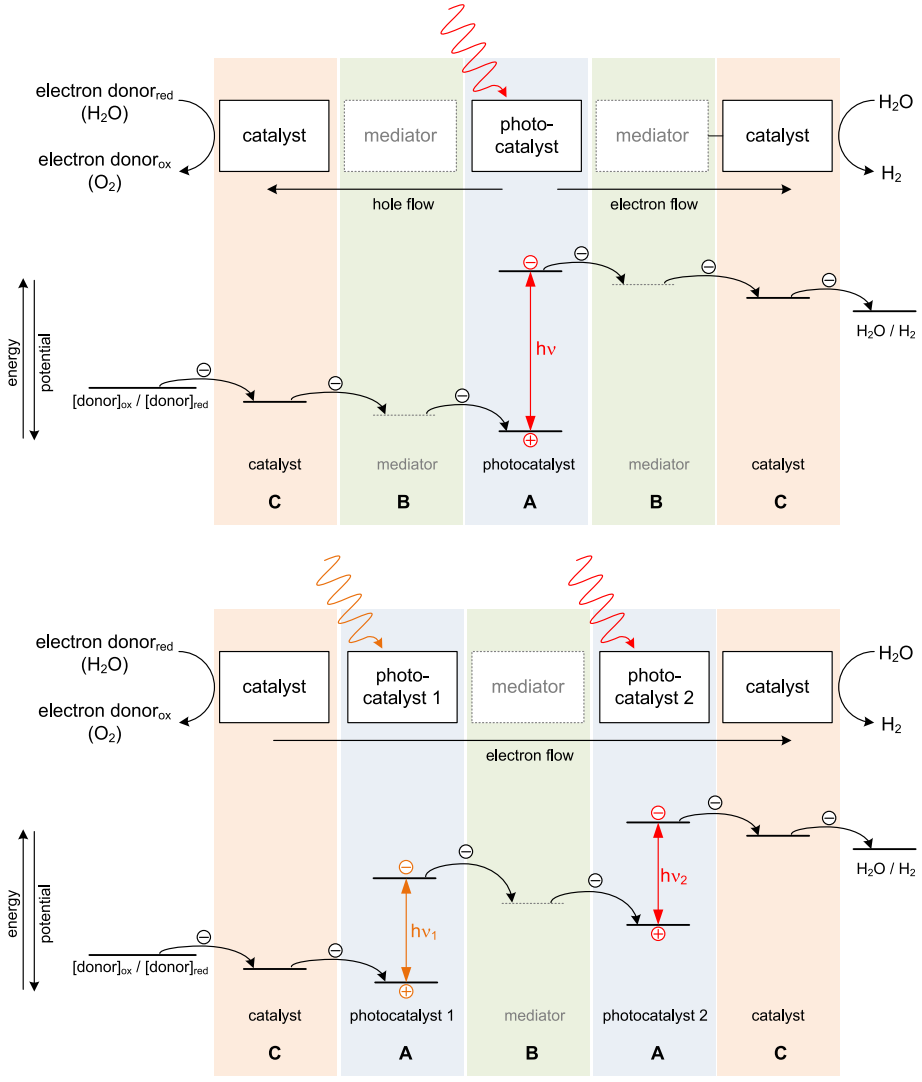

FIGURE 13

Possible roles of coordination compounds in classical (top) and Z-scheme (bottom) photocatalytic water splitting systems: (a) coordination compound as a photocatalyst alone or as a photosensitizer of semiconductor particles; (b) electron shuttling mediator; (c) cocatalyst of water reduction or oxidation. In the classical photocatalytic water splitting system, H_2 and O_2 evolution occur in a single photocatalyst, and electrons and holes flow toward to the opposite side. On the other hand, water oxidation and reduction reactions proceed on the separate photocatalysts and electron flow from O_2 evolution catalyst to H_2 evolution catalyst.

nents in a Z-scheme; or (iii) catalytic sites of a system facilitating the charge collection and water reduction/oxidation. These functionalities of coordination compounds have been summarized in Fig. 13 and will be discussed in the following sections.

Coordination compounds as photosensitizers

Several examples of the application of coordination compounds as photosensitizers of semiconductors were listed in the Section "Oxide photocatalysts for half reactions". Excited complexes adsorbed, or better chemically bound to the semiconductor surface, may inject electrons to the CB or holes to the VB of the semiconductor. In particular, ruthenium complexes may play a role of the photosensitizers.

Application of coordination compounds, particularly with organic ligands, may be associated with a limited overall stability of the photocatalytic systems. Organic ligands may be prone to oxidation by photogenerated holes and/or reactive oxygen species formed in the aqueous media.

Coordination compounds as electron transfer mediators

Transition metal complexes can be also considered as electron-transfer mediators in Z-scheme systems for water splitting. They can be used instead of ionic electron mediators, such as IO_3^-/I^-, $I_3^-/I,^-$ and Fe^{3+}/Fe^{2+}. Unfortunately, these redox couples are not perfectly suited for all Z-scheme systems. Since the early 2000s, some attempts have been made to use metal complexes as redox shuttles in dye-sensitized solar cells (DSSC). Nusbaumer et al. have found that the cobalt redox couple, 2,6-bis(1′-butylbenzimidazol-2′-yl)pyridine ($[Co(dbbip)_2]^{3+/2+}$), offers similar performance as an electron mediator as the well-known I_3^-/I^- redox couple [218]. Also, other cobalt complexes, as well as nickel and iron species, have been found to be active as electron mediators [218–223]. Sasaki et al. were the first who investigated the

effectiveness of cobalt complexes with 1,10-phenanthroline, $[Co(phen)_3]^{3+/2+}$, and 2,2′-bipyridine, $[Co(bpy)_3]^{3+/2+}$, ligands as redox shuttles for visible light-driven Z-scheme photocatalytic systems [46]. In the case of the ($Ru/SrTiO_3$:Rh)–($BiVO_4$) Z-scheme, authors observed that the activity of the $[Co(bpy)_3]^{3+/2+}$ electron mediator system was higher when compared to the activity of $[Co(phen)_3]^{3+/2+}$, whereas in the Ru(0.5 wt%)-decorated $(CuGa)_{0.8}Zn_{0.4}S_2$, $BiVO_4$ photocatalytic system, the cobalt complex with terpyridine $[Co(terpy)_3]^{3+/2+}$ was the most effective mediator [224]. These examples show a flexibility of the used mediators, where a simple change of the ligand can influence properties of the coordinated compound [225]. Although the results are promising, only a few examples were reported and this topic has not been sufficiently explored yet.

There are some analogies between an electron mediator in the Z-scheme photocatalytic system and that in the dye-sensitized solar cell (DSSC). Based on the studies on the use of transition metal complexes as electron-transfer mediators in the DSSC, some conclusions on the possibility of applying them in the Z-scheme systems can be made. Both applications required appropriate redox potentials, good reversibility and an efficient electron transfer through the solid–liquid interface. One of the most studied redox shuttles, in the case of DSSC, is the cobalt (III/II) redox pair. These electron transfer mediators ($[CoL_3]^{3+/2+}$) have several advantages over the ionic redox shuttles based on iodine and iron species. First of all, their redox potentials are easily tunable. Through variation of the ligands the formal potential can be tuned by over 400 mV [226]. Another advantage of the cobalt(III/II) redox shuttles is a low visible light absorption, especially when compared to the I_3^-/I^- couple. On the other hand, these systems have some drawbacks, including a relatively slow mass transport compared to I_3^-/I^- and a high reorganization energy [226]. Also, a relatively low solubility of Co^{3+} complexes causes some problems in charge transportation between two semiconductors [218,221].

Coordination compounds as molecular cocatalysts

Catalysts of water reduction or oxidation may be based not only on metallic or metal oxide nanoparticles, but also on coordination compounds. Such moieties attached to the semiconductor surface exchange electrons (or holes) with the excited photocatalyst and facilitate reduction (or oxidation) of water molecules. Dinuclear iron complexes combined with a semiconductor (e.g., ZnS, MOF (metal organic framework)) were good examples of such systems [227].

The studies on bioinspired diiron catalysts with semiconductors were initiated by Wu and coworkers [228]. A substitution of one CO with other ligands or attachment of other groups to S-bridges were involved to tune catalytic properties of the complex. For instance, a water soluble diiron species in combination with CdTe quantum dots and ascorbate photocatalyzed H_2 production in aqueous solutions at pH 4, with the TON (turnover number) exceeding 500 (calculated for the diiron complex) [228]. The reported TON was further increased by the factor of *ca.* 100 when $[Fe_2(CO)_6(\mu\text{-adt})CH_2C_6H_5]$ (adt = azapropane-1,3-dithiolato) was used as the catalyst together with chitosan constituting a specific surrounding of the active site. The diiron complex $[Fe_2S_2(CO)_6]$, attached to the surface of CdSe QDs in H_2O/CH_2Cl_2, has shown a high TOF (turnover frequency) of 596 h^{-1} when irradiated with a 410-nm LED [4,10,228].

The diiron complex, $[(\mu\text{-SPh-4-}NH_2)_2Fe_2(CO)_6]$, was used to functionalize ZnS as a catalyst for photocatalytic water reduction [229]. An efficient electron transfer from excited ZnS to the adsorbed complex enabled enhancement of the photocatalytic H_2 production in the hybrid system by the factor of approximately 12, compared to ZnS alone using ascorbate as a sacrificial electron donor. The apparent quantum yield of the hydrogen generation reached 2.5% at 325 nm.

A similar approach was employed in the systems utilizing cobalt complexes instead of the diiron moieties. Cobalt coordination compounds (Fig. 14) were combined with CdS, CdSe, CdTe, ZnS, TiO_2 and g-C_3N_4 [227]. In CdS systems the hydrogen evolution reached the quantum yield of 9.1% (at TON = 171) [230], while in the case of CdSe – even 25% at TON = 3×10^5 [231], when cobalt complexes from the families **2** and **3** were involved, respectively. The photocatalytic H_2 evolution was also achieved in cobaloxime–g-C_3N_4 systems, in which TON values reached up to 281 [232].

Beside cobalt and iron complexes also nickel-based coordination compounds can play the role of water reduction cocatalysts. In the system presented in Fig. 15, involving a tris(bipyridine) ruthenium(II) derivative as the photosensitizer of TiO_2 and

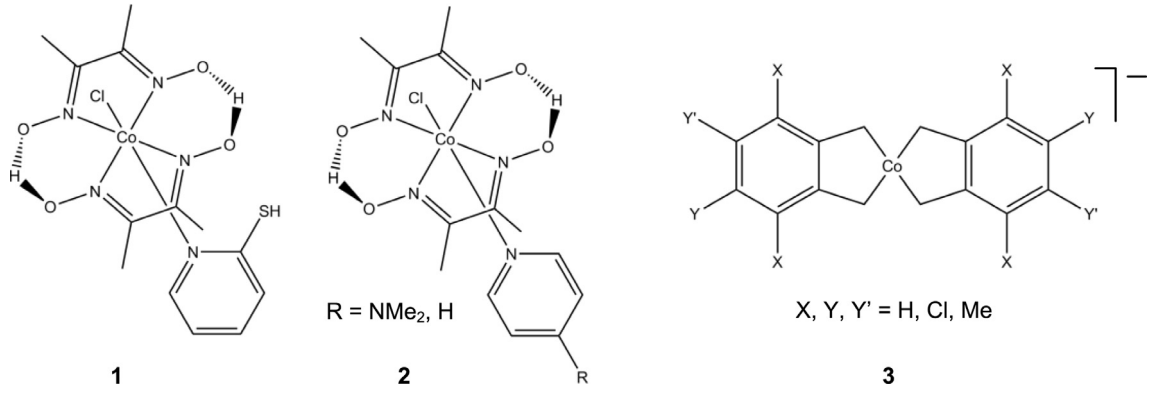

FIGURE 14

Structures of cobalt(III) complexes used as cocatalysts of proton reduction reactions in semiconductor photocatalytic systems.

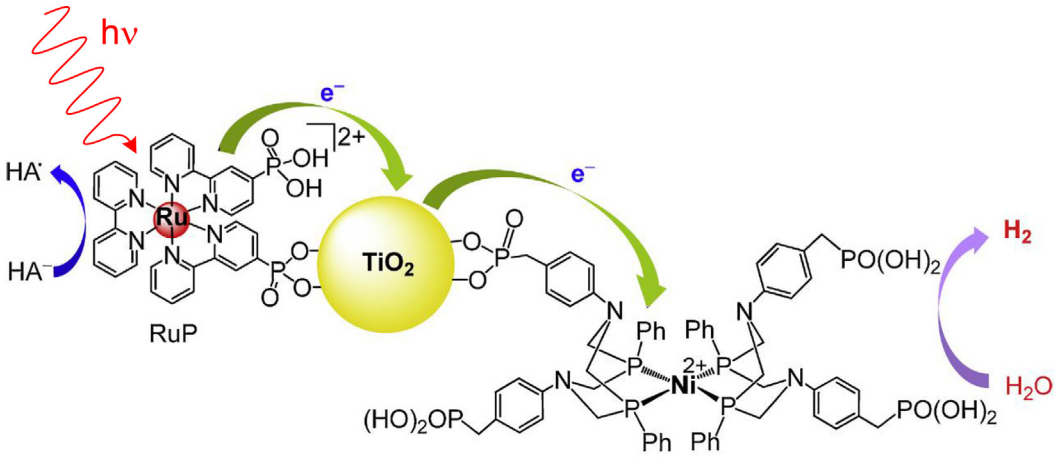

FIGURE 15

Photocatalytic hydrogen production in the system containing TiO_2 photosensitized with the ruthenium complex and covalently bound nickel(II) complex acting as a water reduction catalyst. Reprinted with permission from Ref. [227], Copyright 2015, Elsevier.

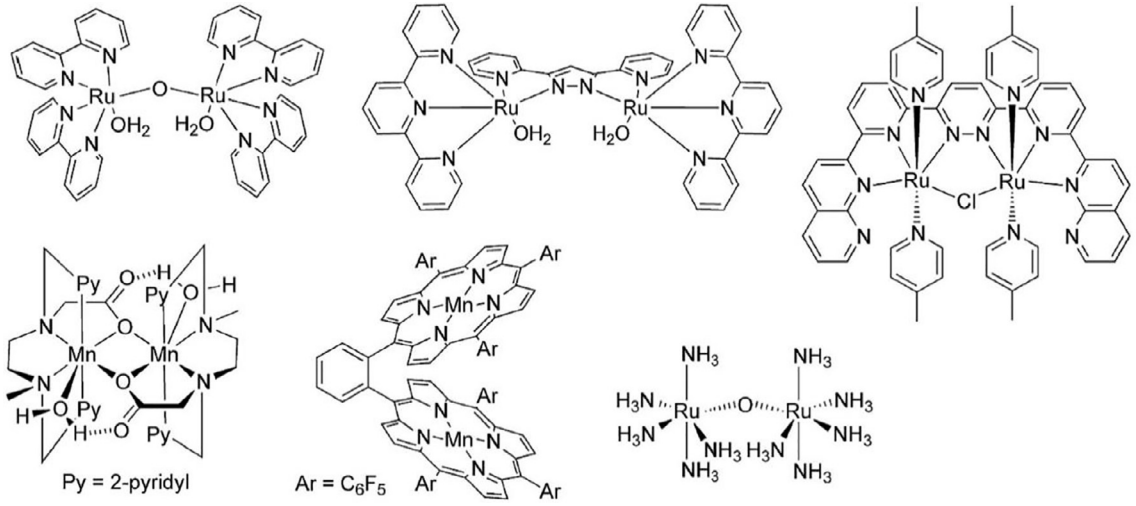

FIGURE 16

Structures of multinuclear manganese and ruthenium complexes facilitating water oxidation.

Ni(II) complex as the cocatalyst the quantum yield efficiency of H_2 production reaches 10% at 460 nm. The main drawback of the system is its low photostability, as photocatalytic degradation of organic ligands takes place in the system.

Water splitting also requires an efficient water oxidation process, which is even more demanding than water reduction [27]. In this half reaction, four holes are involved to produce one O_2 molecule. Coordination compounds can be involved also to catalyze this reaction. Due to the high number of involved electrons (or holes), multinuclear complexes are often considered. They mimic the so-called Oxygen Evolving Complex (OEC) involved in the photosystem II that is based on the $[Mn_4CaO_5]$ core. Possible artificial OECs involve di- and multinuclear complexes with oxygen bridges, like $[(terpy)(H_2O)Mn(\mu\text{-}O)_2Mn(terpy)(H_2O)]^{3+}$, Mn_4O_4 and other multinuclear complexes of manganese [233], ruthenium ($Ru^{III}(\mu\text{-}O)Ru^{III}$) [234], Fe_2O_3 (hematite) [235], cobalt complexes [236,237], mono- and dinuclear Ru(II) complexes with bipyridyl ligands [227,238,239]. Selected structures of OECs are presented in Fig. 16 [240]. Moreover, the multinuclear complexes could realize water oxidation by combining with good stability, durability, and accessibility of heterogeneous metal oxide catalysts. For example, $K_7[Co^{III}Co^{II}(H_2O)W_{11}O_{39}]\cdot 15H_2O$, a Keggin POM composing of only earth-abundant elements (cobalt, tungsten, and oxygen) and a unique mixed-valence Co(III) and Co(II) structural feature, works efficiently and stably for water oxidation under the visible light irradiation [111]. Another typical example to immobilize homogeneous catalysts on the surfaces of heterogeneous materials without losing their reactivity and stability is confining ruthenium molecular catalysts, $[Ru^{II}(bda)(pic)_2]$ (bda: 2,2′-bipyridine-6,6′-dicarboxylate), in the nanocage of SBA-16, which exhibits a significantly higher activity and stability than the corresponding homogeneous catalyst for water oxidation [112]. Above all, the multinuclear complexes somehow combine the advantageous merits of both heterogeneous and homogeneous catalysis, capable to keep the general high efficiency and enhance the stability from the heterogeneous system.

Summary and outlook

Photocatalytic hydrogen and oxygen production based on solar-driven water splitting in a suspension system is one of the most environmental and economic ways to utilize solar energy. Inorganic semiconductors, organic carbon-based photocatalysts and semiconductor-coordination compounds applied in the visible light-driven water splitting systems have a great potential to boost the photocatalyst efficiency to approach the industrial application at large scale.

Oxide materials have the longest history in the studies for the photocatalytic water redox into H_2 and O_2 [3,241], hence they have widely been explored. Essentially, visible light-active photocatalysts, especially native visible light-active photocatalysts, such as $BiVO_4$-, and ABO_3-type photocatalysts, have narrow bandgaps less than 3.0 eV. Non-oxide materials, such as (oxy)nitride and (oxy)sulfide photocatalysts, have the potential to application in overall water splitting as the nitrogen or sulfur atoms replacing oxygen atoms in the crystals could narrow the band gap and increase the light absorption. Typically, the overall water splitting into H_2 and O_2 by solar light is a promising way to generate renewable hydrogen fuel. Among them polyoxometalate ($Ag_3PW_{12}O_{40}$) decorated by carbon quantum dots and silver nanoparticles was efficiently applied for water splitting into H_2 and O_2 under visible light [157], resulting into the high quantum efficiency of 4.9% at the wavelength of 480 nm. In a Z-scheme system, $SrTiO_3$:Rh and $BiVO_4$ mixed with the aqueous Fe^{3+}/Fe^{2+} solution split water into hydrogen and oxygen under visible light illumination as well [46], with the quantum efficiency of 4% at 420 nm. The highly efficient $SrTiO_3$:Rh photocatalysts synthesized by hydrothermal and polymerizable complex methods greatly improved the efficiency for overall water splitting in a Z-scheme system. The so far most efficient Z-scheme is the solid Z-scheme system composed of $SrTiO_3$:La,Rh/C/$BiVO_4$:Mo sheets, which achieved unassisted pure-water splitting with a STH about 1.0% at ambient pressure [175]. Simultaneously, the $SrTiO_3$:La, Rh/Au/$BiVO_4$:Mo sheets are also competitive candidates for realizing the overall water splitting under visible light irradiation, which exhibited an AQY of 33% at 419 nm and an STH of 1.1% in overall pure water splitting [174].

Whereas, most of these inorganic semiconductors are highly stable and robust, they are often barely tunable [215]. Although inorganic photocatalysts dominated the field of photocatalytic water splitting in the past decades, organic semiconductors are emerging as effective photocatalysts with increasing fascinating opportunities because the structures and properties of organic photocatalysts can be easily tailored. Many metal-free or organic photocatalysts, including carbon nitride, GO, heteroatom-doped graphene, boron carbide, *h*-BCN, conjugated polymer, and supramolecular organic system, have been designed and preliminarily tested in water splitting with visible light irradiation. The photocatalytic water splitting activity of these organic photocatalysts will be significantly improved by taking advantage of the protocols of molecular design and band structure engineering.

Coordination compounds in Z-scheme water splitting systems could work alone as a photocatalyst, or a photosensitizer, an electron shuttling mediator, or a cocatalyst of water reduction/oxidation. For example, ruthenium complexes [118] are particularly applied as the photosensitizers to be excited by the visible light, leading to electron transfer to the adherent semiconductors. Transition metal complexes, cobalt complexes, and nickel and iron species have been found to be active as electron mediators in a Z-scheme overall water splitting system.

The target of solar energy conversion efficiency by photocatalytic and photoelectrochemical water splitting was predicted at 10% for approximately 10,000 "solar plants" (5 km * 5 km in area per plant) to satisfy one-third of the projected energy needs of human society in 2050 [176]. Correspondingly, it is necessary to achieve 30% quantum yield at 600 nm of water splitting into H_2 and O_2 [26], then the efficiency gives about 5% of solar energy to hydrogen fuel. The current benchmark quantum yield is far away from this target although tremendous progress has been achieved in the field of the photocatalytic water splitting into hydrogen and oxygen under visible light irradiation in a suspension system. The $SrTiO_3$:La, Rh/Au/$BiVO_4$:Mo and $SrTiO_3$: La, Rh/C/$BiVO_4$:Mo sheets are approaching this target but the quantum yield is still low. Therefore, there is more work to be fulfilled in the future. Firstly, the exploration of simple, inexpensive, large-scale and reproducible photocatalysts and subtle control of their composition, crystallinity and microstructure are vital for increasing the light absorption, charge transfer, and active sites, simultaneously preventing the charge carriers' recombination. Secondly, it is anticipated to explore and broaden the applications of these photocatalysts in the solar energy conversion, including water splitting (even for overall water splitting without any sacrificial agent), CO_2 reduction, environmental remediation, and ammonia synthesis. Third, device fabrication, equivalent to material discovery, should be paid attention as it has hardly been investigated. Finally, the investigation of charge-carrier dynamics, the nature of the catalytically active sites and reaction intermediates will be required to fully understand the photocatalytic process at molecular level, which can further boost the efficiency of these photocatalysts and make them practically viable. In total, photocatalytic water splitting is still at early stage. Substantial efforts are required to push it forward and coordination between material science, photochemistry, photophysics, and engineering is crucial to achieve the minimum threshold of 10% solar to fuel conversion efficiency.

Acknowledgments

D. K. would like to thank the CSC for Ph.D. funding. Y. W. and J. T. acknowledges financial support from EPSRC (EP/N009533/1), Leverhulme Trust (Grant No: RPG-2017-122) and Royal Society-Newton Advanced Fellowship grant (NA170422). Y. Z. and X. C. W. thanks the financial supports from National Basic Research Program of China (2013CB632405), the National Natural Science Foundation of China (21425309) and the 111 Project. W. M. and M. K. thank the National Science Center in Poland for the support (Project No. 2015/19/B/ST5/00950).

Appendix A. Supplementary data

Supplementary data associated with this article can be found, in the online version, at https://doi.org/10.1016/j.mattod.2018.04.009.

References

[1] S.J.A. Moniz et al., Environ. Sci. 8 (3) (2015) 731.
[2] D.J. Martin et al., Chem. Soc. Rev. 44 (21) (2015) 7808.
[3] A. Fujishima, K. Honda, Nature 238 (5358) (1972) 37.
[4] Z. Li et al., Environ. Sci. 6 (2) (2013) 347.
[5] M. Ni et al., Renew. Sust. Energ. Rev. 11 (3) (2007) 401.
[6] S.U.M. Khan et al., Science 297 (5590) (2002) 2243.
[7] K. Maeda et al., J. Am. Chem. Soc. 127 (23) (2005) 8286.
[8] X. Yang et al., Nano Lett. 9 (6) (2009) 2331.
[9] D. Hwang et al., Catal. Lett. 80 (1–2) (2002) 53.
[10] F. Wang et al., J. Phys. Chem. C 116 (16) (2012) 8901.
[11] A. Kleiman-Shwarsctein et al., J. Phys. Chem. C 112 (40) (2008) 15900.
[12] I. Cesar et al., J. Am. Chem. Soc. 128 (14) (2006) 4582.
[13] M. Sathish et al., Int. J. Hydrogen Engerg. 31 (7) (2006) 891.
[14] N. Bao et al., Chem. Mater. 20 (1) (2008) 110.
[15] S. Wu et al., J. Phys. Chem. C 113 (41) (2009) 17893.
[16] S. Liu et al., ACS Appl. Mater. Inter. 6 (4) (2014) 2407.
[17] V.R. Reddy et al., Korean J. Chem. Eng. 20 (6) (2003) 1026.
[18] T. Kodama et al., Sol. Energy 78 (5) (2005) 623.
[19] R. Abe et al., J. Am. Chem. Soc. 132 (34) (2010) 11828.
[20] M. Higashi et al., Chem. Lett. 37 (2) (2008) 138.
[21] S.Y. Tee et al., Adv. Sci. 4 (5) (2017) 1600337.
[22] S. Chen et al., Nat. Rev. Mater. 2 (2017) 17050.
[23] K. Takanabe, ACS Catal. 7 (11) (2017) 8006.
[24] A. Kudo, M. Sekizawa, Chem. Commun. 15 (2000) 1371.
[25] M. Liu et al., Chem. Commun. 19 (2004) 2192.
[26] A. Kudo, Y. Miseki, Chem. Soc. Rev. 38 (1) (2009) 253.
[27] J. Tang et al., J. Am. Chem. Soc. 130 (42) (2008) 13885.
[28] A. Kubacka et al., Chem. Rev. 112 (3) (2012) 1555.
[29] F.M. Pesci et al., J. Phys. Chem. C. Nanomater. Interfaces 117 (48) (2013) 25837.
[30] M. Reza Gholipour et al., Nanoscale 7 (18) (2015) 8187.
[31] H. Ahmad et al., Renew. Sust. Energ. Rev. 43 (2015) 599.
[32] A. Primo et al., PCCP 13 (3) (2011) 886.
[33] K. Qi et al., J. Catal. 38 (12) (2017) 1936.
[34] S. Okunaka et al., J. Mater. Chem. A 3 (28) (2015) 14794.
[35] F. Cai et al., RSC Adv. 5 (71) (2015) 57354.
[36] L. Wang et al., Fuel 140 (2015) 267.
[37] K. Maeda, ACS Appl. Mater. Inter. 6 (3) (2014) 2167.
[38] W. Yan et al., J. Phys. Chem. C 118 (12) (2014) 6077.
[39] Z.-F. Huang et al., J. Am. Chem. Soc. 138 (4) (2016) 1359.
[40] A.D. Handoko et al., Curr. Opin. Chem. Eng. 2 (2) (2013) 200.
[41] H. Xu et al., J. Phys. Chem. B 110 (28) (2006) 13829.
[42] L. Pan et al., ACS Appl. Mater. Inter. 4 (3) (2012) 1650.
[43] H. Kato et al., J. Am. Chem. Soc. 125 (10) (2003) 3082.
[44] Y.-S. Hu et al., Chem. Mater. 20 (12) (2008) 3803.
[45] Z. Zou et al., Nature 414 (6864) (2001) 625.
[46] H. Kato et al., J. Mater. Chem. A 1 (39) (2013) 12327.
[47] K. Maeda et al., ACS Catal. 3 (5) (2013) 1026.
[48] R. Niishiro et al., Appl. Catal. B: Environ. 150–151 (2014) 187.
[49] K. Kawashima et al., J. Phys. Chem. C 119 (28) (2015) 15896.
[50] T. Hisatomi et al., Environ. Sci. 6 (12) (2013) 3595.
[51] S.S.K. Ma et al., J. Am. Chem. Soc. 134 (49) (2012) 19993.
[52] D.J. Martin et al., J. Am. Chem. Soc. 136 (36) (2014) 12568.
[53] X. Li et al., Adv. Mater. 28 (12) (2016) 2427.
[54] X.-F. Yang et al., Accounts Chem. Res. 46 (8) (2013) 1740.
[55] J. Xing et al., Chemistry A Eur. J. 20 (8) (2014) 2138.
[56] P. Yin et al., Angew. Chem. Int. Ed. 55 (36) (2016) 10800.
[57] H. Fei et al., Nat. Commun. 6 (2015) 8668.
[58] N. Cheng et al., Nat. Commun. 7 (2016) 13638.
[59] K. Hideki et al., B. Chem. Soc. JPN. 80 (12) (2007) 2457.
[60] B.P. Nelson et al., Langmuir 16 (15) (2000) 6094.
[61] L.A. Lyon, J.T. Hupp, J. Phys. Chem. B 103 (22) (1999) 4623.
[62] R. Abe et al., J. Phys. Chem. B 109 (33) (2005) 16052.
[63] J.F. Callejas et al., ACS Nano 8 (11) (2014) 11101.
[64] J. Tian et al., J. Am. Chem. Soc. 136 (21) (2014) 7587.
[65] Y. Shi, B. Zhang, Chem. Soc. Rev. 45 (6) (2016) 1529.
[66] A. Ghicov, P. Schmuki, Chem. Commun. (20) (2009) 2791.
[67] J.J. Gooding, Electrochim. Acta 50 (15) (2005) 3049.
[68] X. Chen et al., Chem. Rev. 110 (11) (2010) 6503.
[69] X. Chen et al., Science 331 (6018) (2011) 746.
[70] S.N. Tijare et al., Int. J. Hydrogen Engerg. 37 (13) (2012) 10451.
[71] K. Maeda et al., ACS Catal. 5 (3) (2015) 1700.
[72] W. Zhang et al., J. Am. Chem. Soc. 133 (51) (2011) 20680.
[73] I. Tsuji et al., Chem. Mater. 18 (7) (2006) 1969.
[74] I. Tsuji et al., J. Am. Chem. Soc. 126 (41) (2004) 13406.
[75] J.S. Jang et al., Catal. Today 120 (2) (2007) 174.
[76] X. Xu et al., Nat. Mater. 11 (7) (2012) 595.
[77] F.A. Frame et al., J. Am. Chem. Soc. 133 (19) (2011) 7264.
[78] B. Wang et al., Appl. Catal. B: Environ. 166–167 (2015) 320.
[79] R. Li et al., Environ. Sci. 7 (4) (2014) 1369.
[80] K. Tsuji et al., ChemSusChem 9 (16) (2016) 2201.
[81] P. Zhou et al., Adv. Mater. 26 (29) (2014) 4920.
[82] K. Maeda et al., J. Phys. Chem. C 115 (7) (2011) 3057.
[83] C. Gomes Silva et al., J. Am. Chem. Soc. 133 (3) (2011) 595.
[84] J. Ran et al., Chem. Soc. Rev. 43 (22) (2014) 7787.
[85] H. Li et al., Adv. Sci. 3 (11) (2016) 1500389.
[86] W. Erbs et al., J. Phys. Chem. 88 (18) (1984) 4001.
[87] D. Xu et al., Langmuir (2015).
[88] T. Puangpetch et al., J. Mol. Catal. A: Chem. 312 (1–2) (2009) 97.
[89] D. Ke et al., Appl. Catal. A: Gen. 350 (1) (2008) 111.
[90] A. Mukherji et al., J. Phys. Chem. C 115 (31) (2011) 15674.
[91] H. Yu et al., J. Mater. Chem. A 2 (10) (2014) 3344.
[92] B. Liu et al., Environ. Sci. 7 (8) (2014) 2592.
[93] S. Martha et al., J. Mater. Chem. A 2 (10) (2014) 3621.
[94] K.H. Reddy et al., RSC Adv. 2 (25) (2012) 9423.
[95] K.M. Parida et al., Dalton T. 40 (48) (2011) 12839.
[96] A. Nashim et al., ChemCatChem 5 (8) (2013) 2352.
[97] K. Ding et al., J. Mater. Chem. A 2 (22) (2014) 8294.
[98] R. Li et al., Nat. Commun. 4 (2013) 1432.
[99] L. Duan et al., Nat. Chem. 4 (2012) 418.
[100] N. Kaveevivitchai et al., J. Am. Chem. Soc. 134 (26) (2012) 10721.
[101] N.D. McDaniel et al., J. Am. Chem. Soc. 130 (1) (2008) 210.
[102] J.F. Hull et al., J. Am. Chem. Soc. 131 (25) (2009) 8730.
[103] N.S. McCool et al., J. Am. Chem. Soc. 133 (30) (2011) 11446.
[104] C.-F. Leung et al., Environ. Sci. 5 (7) (2012) 7903.
[105] D. Hong et al., Environ. Sci. 5 (6) (2012) 7606.
[106] Y.V. Geletii et al., Angew. Chem. Int. Ed. 47 (21) (2008) 3896.
[107] A. Sartorel et al., J. Am. Chem. Soc. 130 (15) (2008) 5006.
[108] Y.V. Geletii et al., J. Am. Chem. Soc. 131 (22) (2009) 7522.
[109] S. Tanaka et al., Chem. Commun. 48 (11) (2012) 1653.
[110] M. Murakami et al., J. Am. Chem. Soc. 133 (30) (2011) 11605.
[111] F. Song et al., Environ. Sci. 6 (4) (2013) 1170.
[112] B. Li et al., Environ. Sci. 5 (8) (2012) 8229.
[113] C. Yin et al., J. Mater. Chem. A 1 (29) (2013) 8367.
[114] W.J. Jo et al., Angew. Chem. Int. Ed. 51 (13) (2012) 3147.
[115] W. Yao et al., Dalton T. 11 (2008) 1426.
[116] Y. Li et al., J. Mol. Catal. A: Chem. 282 (1–2) (2008) 117.
[117] L. Qi et al., PCCP 13 (19) (2011) 8915.
[118] W. Kim et al., J. Phys. Chem. C 113 (24) (2009) 10603.
[119] K. Maeda et al., J. Phys. Chem. C 113 (18) (2009) 7962.
[120] W. Kim et al., Environ. Sci. 3 (11) (2010) 1789.
[121] W. Cui et al., Catal. Today 207 (2013) 44.
[122] X. Zhang et al., RSC Adv. 3 (34) (2013) 14363.
[123] W. Cui et al., Chem. Eng. J. 204–206 (2012) 1.
[124] B. O'Regan, M. Gratzel, Nature 353 (6346) (1991) 737.
[125] S.H. Ko et al., Nano Lett. 11 (2) (2011) 666.
[126] P. Wang et al., Nat. Mater. 2 (6) (2003) 402.
[127] M. Law et al., Nat. Mater. 4 (6) (2005) 455.
[128] U. Bach et al., Nature 395 (6702) (1998) 583.
[129] R. Sasaki et al., Appl. Catal. B: Environ. 128 (2012) 72.
[130] S. Min Ji et al., PCCP 7 (6) (2005) 1315.
[131] K. Maeda et al., B. Chem. Soc. JPN. 81 (8) (2008) 927.
[132] M. Hojamberdiev et al., Cryst. Growth Des. 15 (9) (2015) 4663.
[133] S. Ida et al., J. Am. Chem. Soc. 134 (38) (2012) 15773.
[134] S. Balaz et al., Chem. Mater. 25 (16) (2013) 3337.
[135] W. Wang et al., Prog. Mater Sci. (2017).
[136] A. Rachel et al., Thermochim. Acta 438 (1) (2005) 134.
[137] Y. Moriya et al., Chem. Rev. 257 (13) (2013) 1957.
[138] Y. Mori et al., J. Cryst. Growth 350 (1) (2012) 72.
[139] J.K. Jian et al., J. Cryst. Growth 291 (1) (2006) 72.
[140] S. Shen et al., J. Phys. Chem. C 112 (41) (2008) 16148.
[141] M. Tabata et al., J. Phys. Chem. C 114 (25) (2010) 11215.
[142] H. Wang et al., Int. J. Hydrogen Engerg. 40 (1) (2015) 340.
[143] S. Peng et al., Int. J. Hydrogen Engerg. 37 (2) (2012) 1366.

[144] K. Li et al., ACS Catal. 3 (2) (2013) 170.
[145] B. Chai et al., J. Mater. Chem. 21 (38) (2011) 14587.
[146] X. Zong et al., Chem. Commun. 30 (2009) 4536.
[147] X. Zong et al., J. Am. Chem. Soc. 130 (23) (2008) 7176.
[148] A. Ishikawa et al., J. Am. Chem. Soc. 124 (45) (2002) 13547.
[149] F. Zhang et al., Chem. Commun. 46 (39) (2010) 7313.
[150] T. Suzuki et al., PCCP 14 (44) (2012) 15475.
[151] K. Ogisu et al., J. Phys. Chem. C 112 (31) (2008) 11978.
[152] O. Kiyonori et al., Chem. Lett. 36 (7) (2007) 854.
[153] H. Yan et al., J. Catal. 266 (2) (2009) 165.
[154] T. Takata et al., Res. Chem. Intermediat. 33 (1) (2007) 13.
[155] K. Maeda et al., Nature 440 (7082) (2006) 295.
[156] T. Ohno et al., J. Am. Chem. Soc. 134 (19) (2012) 8254.
[157] J. Liu et al., ChemCatChem 6 (9) (2014) 2634.
[158] K. Maeda et al., Chemistry A Eur. J. 19 (16) (2013) 4986.
[159] Y. Lee et al., J. Phys. Chem. C 111 (2) (2007) 1042.
[160] M. Hara et al., Chem. Commun. 3 (1998) 357.
[161] K. Maeda et al., Angew. Chem. Ger. Edit. 122 (24) (2010) 4190.
[162] T.-F. Yeh et al., Adv. Mater. 26 (20) (2014) 3297.
[163] C. Zhu et al., Appl. Catal. B: Environ. 216 (2017) 114.
[164] W. Shi et al., J. Mater. Chem. A 5 (37) (2017) 19800.
[165] C. Yan et al., Nano Energy 39 (2017) 539.
[166] L. Zhang et al., Chemistry A Eur. J. 21 (50) (2015) 18089.
[167] Q. Jia et al., Chem. Sci. 5 (4) (2014) 1513.
[168] Q. Wang et al., Chem. Mater. 26 (14) (2014) 4144.
[169] M. Higashi et al., Chem. Mater. 21 (8) (2009) 1543.
[170] Y. Sasaki et al., J. Am. Chem. Soc. 135 (14) (2013) 5441.
[171] R. Abe et al., Chem. Commun. 24 (2009) 3577.
[172] M. Tabata et al., Langmuir 26 (12) (2010) 9161.
[173] S. Hara et al., J. Phys. Chem. C 116 (33) (2012) 17458.
[174] Q. Wang et al., Nat. Mater. 15 (6) (2016) 611.
[175] Q. Wang et al., J. Am. Chem. Soc. 139 (4) (2017) 1675.
[176] K. Maeda, K. Domen, J. Phys. Chem. Lett. 1 (18) (2010) 2655.
[177] L. Li et al., J. Am. Chem. Soc. 138 (24) (2016) 7681.
[178] X. Wang et al., J. Am. Chem. Soc. 131 (5) (2009) 1680.
[179] Y. Li et al., Adv. Mater. 28 (32) (2016) 6959.
[180] Y. Cao et al., Angew. Chem. Int. Ed. 56 (40) (2017) 12191.
[181] Q. Han et al., ACS Nano 10 (2) (2016) 2745.
[182] D. Liu et al., Adv. Mater. 28 (33) (2016) 7284.
[183] G. Zhang et al., Angew. Chem. Int. Ed. 55 (51) (2016) 15712.
[184] D. Zheng et al., Angew. Chem. Int. Ed. 55 (38) (2016) 11512.
[185] G. Liu et al., Angew. Chem. Ger. Edit. 127 (46) (2015) 13765.
[186] M. Zhang, X. Wang, Environ. Sci. 7 (6) (2014) 1902.
[187] D. Zheng et al., Chem. Commun. 51 (98) (2015) 17467.
[188] J. Ran et al., Environ. Sci. 8 (12) (2015) 3708.
[189] H. Yan, Y. Huang, Chem. Commun. 47 (14) (2011) 4168.
[190] Q. Gu et al., Small 12 (26) (2016) 3543.
[191] L. Sun et al., Adv. Funct. Mater. 26 (27) (2016) 4943.
[192] Y. Kang et al., Adv. Mater. 28 (30) (2016) 6471.
[193] D.J. Martin et al., Angew. Chem. Int. Ed. 53 (35) (2014) 9240.
[194] G. Zhao et al., Sci. Technol. 5 (6) (2015) 3416.
[195] J. Yan et al., Appl. Catal. B: Environ. 191 (2016) 130.
[196] H.L. Gao et al., PCCP 15 (41) (2013) 18077.
[197] M.K. Bhunia et al., Chem. Mater. 27 (24) (2015) 8237.
[198] L. Lin et al., ACS Catal. 6 (6) (2016) 3921.
[199] M. Döblinger et al., Chem. Commun. (2009) 1541.
[200] D. Dontsova et al., Chem. Mater. 27 (15) (2015) 5170.
[201] D. Dontsova et al., Chem. Mater. 28 (3) (2016) 772.
[202] Y. Ham et al., Chem. Asian J. 8 (1) (2013) 218.
[203] M.K. Bhunia et al., Angew. Chem. Int. Ed. 53 (41) (2014) 11001.
[204] L. Stegbauer et al., Chem. Sci. 5 (7) (2014) 2789.
[205] Y. Xu et al., Chem. Soc. Rev. 45 (11) (2016) 3039.
[206] T.F. Yeh et al., Adv. Funct. Mater. 20 (14) (2010) 2255.
[207] T.-F. Yeh et al., J. Phys. Chem. C 117 (13) (2013) 6516.
[208] M. Latorre-Sánchez et al., Angew. Chem. Int. Ed. 52 (45) (2013) 11813.
[209] J. Liu et al., Angew. Chem. Int. Ed. 52 (11) (2013) 3241.
[210] C. Huang et al., Nat. Commun. 6 (2015) 7698.
[211] R.S. Sprick et al., Angew. Chem. Int. Ed. 55 (5) (2016) 1792.
[212] K. Kailasam et al., Macromol. Rapid Comm. 34 (12) (2013) 1008.
[213] R.S. Sprick et al., J. Am. Chem. Soc. 137 (9) (2015) 3265.
[214] C. Yang et al., Angew. Chem. Int. Ed. 55 (32) (2016) 9202.
[215] V.S. Vyas, B.V. Lotsch, Nature 521 (2015) 41.
[216] J. Thote et al., Chemistry A Eur. J. 20 (48) (2014) 15961.
[217] L. Wang et al., Adv. Mater. 29 (38) (2017) 1702428.
[218] H. Nusbaumer et al., J. Phys. Chem. B 105 (43) (2001) 10461.
[219] S.A. Sapp et al., J. Am. Chem. Soc. 124 (37) (2002) 11215.
[220] T.C. Li et al., J. Am. Chem. Soc. 132 (13) (2010) 4580.
[221] H. Nusbaumer et al., Chem. Eur. J. 9 (16) (2003) 3756.
[222] B.A. Gregg et al., J. Phys. Chem. B 105 (7) (2001) 1422.
[223] H. Xiang et al., ChemSusChem 10 (5) (2017) 938.
[224] T. Kato et al., J. Phys. Chem. Lett. 6 (6) (2015) 1042.
[225] K. Szaciłowski et al., Coord. Chem. Rev. 208 (1) (2000) 277.
[226] T.W. Hamann, Dalton T. 41 (11) (2012) 3111.
[227] M. Wang et al., Coordin. Chem. Rev. 287 (Suppl. C) (2015) 1.
[228] F. Wang et al., Angew. Chem. Int. Ed. 50 (14) (2011) 3193.
[229] F. Wen et al., ChemSusChem 5 (5) (2012) 849.
[230] F. Wen et al., J. Catal. 281 (2) (2011) 318.
[231] A. Das et al., Proc. Natl. Acad. Sci. U. S. A. 110 (2013) 16716.
[232] X.-W. Song et al., RSC Adv. 4 (36) (2014) 18853.
[233] K.J. Young et al., Acc. Chem. Res. 48 (2015) 567–574.
[234] H. Yamazaki et al., Coord. Chem. Rev. 254 (2010) 2483.
[235] M.J. Katz et al., Coord. Chem. Rev. 256 (2012) 2521.
[236] S.Y. Reece et al., Science 334 (2011) 645.
[237] J.G. McAlpina et al., Coord. Chem. Rev. 256 (2012) 2445.
[238] W. Rabten et al., Inorg. Chem. 54 (2015) 4611–4620.
[239] M. Hirahara et al., Inorg. Chem. 54 (15) (2015) 7627.
[240] T. Kikuchi, K. Tanaka, Eur. J. Inorg. Chem. 2014 (4) (2014) 607.
[241] J.H. Carey et al., B. Environ. Contam. Tox. 16 (6) (1976) 697.